The Abdus Salam
International Centre for Theoretical Physics

United Nations
Educational, Scientific
and Cultural Organization

International Atomic
Energy Agency

H4.SMR/1645-16

"2nd Workshop on Earthquake Engineering for Nuclear Facilities: Uncertainties in Seismic Hazard"

14 - 25 February 2005

Active faulting and natural hazards in Aremenia, eastern Turkey and northwestern Iran

A. S. Karakhanian

Georisk Scientific Research Company
Yerevan, Armenia

Available online at www.sciencedirect.com
SCIENCE DIRECT
Tectonophysics 380 (2004) 189–219
TECTONOPHYSICS
www.elsevier.com/locate/tecto

Active faulting and natural hazards in Armenia, eastern Turkey and northwestern Iran

Arkady S. Karakhanian[a,*], Vladimir G. Trifonov[b], Herve Philip[c], Ara Avagyan[a], Khaled Hessami[d], Farshad Jamali[e], M. Salih Bayraktutan[f], H. Bagdassarian[a], S. Arakelian[a], V. Davtian[a], A. Adilkhanyan[a]

[a] *GEORISK Scientific Research Company, 24a Baghramian Avenue, Yerevan 375019, Armenia*
[b] *Geological Institute of the Russian Academy of Sciences, 7 Pyzhevsky, Moscow 109017, Russia*
[c] *Laboratory of Geophysics, Tectonics and Sedimentology, UMR 5573, Montpellier-2 University, France*
[d] *International Institute of Earthquake Engineering and Seismology, Tehran, Iran*
[e] *MOSHANIR Power Engineering Consultants, P.O. Box 19395-4691, Tehran, Iran*
[f] *Ataturk University, Erzerum, Turkey*

Received 26 April 2002; accepted 28 September 2003

Abstract

Active fault zones of Armenia, SE Turkey and NW Iran present a diverse set of interrelated natural hazards. Three regional case studies in this cross-border zone are examined to show how earthquakes interact with other hazards to increase the risk of natural disaster. In northern Armenia, a combination of several natural and man-made phenomena (earthquakes, landslides and unstable dams with toxic wastes) along the Pambak-Sevan-Sunik fault (PSSF) zone lowers from 0.4 to 0.2–0.3*g* the maximum permissible level (MPL) of seismic hazard that may induce disastrous destruction and loss of life in the adjacent Vanadzor depression.

In the Ararat depression, a large active fault-bounded pull-apart basin at the junction of borders of Armenia, Turkey, Iran and Azerbaijan, an earthquake in 1840 was accompanied by an eruption of Ararat Volcano, lahars, landslides, floods, soil subsidence and liquefaction. The case study demonstrates that natural hazards that are secondary with respect to earthquakes may considerably increase the damage and the casualties and increase the risk associated with the seismic impact.

The North Tabriz–Gailatu fault system poses a high seismic hazard to the border areas of NW Iran, eastern Turkey, Nakhichevan (Azerbaijan) and southern Armenia. Right-lateral strike–slip motions along the North Tabriz fault have given rise to strong earthquakes, which threaten the city of Tabriz with its population of 1.2 million.

The examples illustrate how the concentration of natural hazards in active fault zones increases the risk associated with strong earthquakes in Armenia, eastern Turkey and NW Iran. This generally occurs across the junctions of international borders. Hence, the transboundary character of active faults requires transboundary cooperation in the study and mitigation of the natural risk.

Keywords: Active faults; Earthquakes; Paleoseismicity; Holocene volcanism; Landslides

* Corresponding author. Tel.: +374-1-522344, +374-1-526517; fax: +374-1-565626.
E-mail address: georisk@sci.am (A.S. Karakhanian).

0040-1951/$ - see front matter © 2003 Elsevier B.V. All rights reserved.
doi:10.1016/j.tecto.2003.09.020

1. Introduction

The Armenian Uplands have been one of the test sites for developing principles and practices of active fault studies in the framework of the ILP Project II-2 *World Map of Major Active Faults*, PICS-417 and others. The general pattern and characteristics of active faults in the region were described in our earlier publications (Karakhanian et al., 1997a,b, 2002; Trifonov et al., 1994, 1996; Rebai et al., 1993; Philip et al., 1989, 1992, 2001; and others). In this paper, we present new data and update the earlier results in order to review natural hazards related to fault activity. These hazards include not only strong earthquakes, but also volcanism, landslides and environmental changes (ground deformation, hydrogeological and landscape changes). These related hazards often accompany strong earthquakes, but can also result from tectonic creep on fault zones.

Armenia, SE Turkey and NW Iran are in the central part of the Arabian lithospheric collisional zone, a region which experiences N–S shortening and E–W extension accompanied by intense faulting, strong earthquakes and active volcanism (Dewey et al., 1986; Taymaz, 1991). As a result of convergence of the Arabian and Eurasian plates, the Anatolian block is being ejected westward, and the Iranian block forced eastward. The Arabian–Eurasian convergence occurs at a rate of 28–37 mm/year (NUVEL-1A, De Mets et al., 1990), but the average shortening estimates suggest that 80–90% of the deformation is aseismic (Chase, 1978; Minster and Jordan, 1978; Shoja-Taheri and Niazi, 1981; Jackson and McKenzie, 1988; De Mets et al., 1990). Recently, GPS data have imposed bounds on the regional strain rates across this region, indicating crustal shortening rates of 10 ± 2 mm/year (Reilinger and Barka, 1997).

The North Anatolian, East Anatolian, Levant, Zagros, Alborz and other active faults on the flanks of the Arabian collision zone define the blocks of Anatolia and Iran. These faults are each from 700 to 1700 km long and are characterized by horizontal slip rates of 7–30 mm/year (Ambraseys and Jackson, 1998). Numerous strong earthquakes (M=7.5–7.7) with recurrence intervals of several hundreds of years have been associated with these faults (Jackson and McKenzie, 1988; Ambraseys and Melville, 1982; Ambraseys and Jackson, 1998; Reilinger and Barka, 1997).

Armenia, eastern Turkey and northwestern Iran are in the central part of the collision zone. Manifestations of geodynamic and seismic activity are contrasting and complex in this region and still poorly understood. There is still no clear estimate of maximum expected magnitudes and recurrence intervals of earthquakes on the numerous active strike–slip and reverse faults in the region. M=7.2–7.5 earthquakes are associated with these faults, although their individual lengths do not exceed 350–500 km and slip rates vary from 4 to 0.5 mm/year (Nikonov and Nikonova, 1986; Trifonov et al., 1994; Philip et al., 2001; Berberian, 1994, 1997; Guidoboni and Traina, 1995, 1996; Shebalin et al., 1997; Karakhanian et al., 1997a, b, 2002).

In northern Armenia, eastern Turkey and northwestern Iran, the faults form a northward-bending structural arc (Fig. 1). Within the arc, deformation is characterized by E–W-striking reverse and thrust faults, oblique strike–slip faults, as well as N–S-striking normal faults. The outer part of the arc is defined by two active faults: Zheltorechensk-Sarighamish Fault (ESF) and Pambak-Sevan-Sunik fault (PSSF). The Zheltorechensk-Sarighamish fault is a left-lateral strike–slip structure, and the Pambak-Sevan-Sunik fault is right-lateral strike–slip fault. The inner part of the arc is defined by the left-lateral strike–slip Akhourian fault (AF), and right-lateral strike–slip Garni fault (GF). The inner pair of faults link with the outer part of the arc at its northwestern end. The southern part of the arc terminates by the active faults that border the Ararat Valley, including Sardarapat fault (SF), Nakhichevan fault (NF), Dogubayazet fault (DF), Maku (MF), Gailatu–Siah Cheshmeh–Khoy fault (GSKF) and other faults shown in Fig. 1.

A number of publications describe the main characteristics of these faults (Trifonov et al., 1990; Philip et al., 1989; Rebai et al., 1993; Trifonov et al., 1994; Berberian, 1981, 1994, 1997; Karakhanian, 1993; Karakhanian et al., 1997b; Philip et al., 2001). However, many aspects of geometry, kinematics, and slip rates of these faults are still unclear: consequently, assessments of their seismic hazard are uncertain. This is particularly so in the border zone at the junction of Armenia, Azerbaijan, Turkey and Iran. Our limited

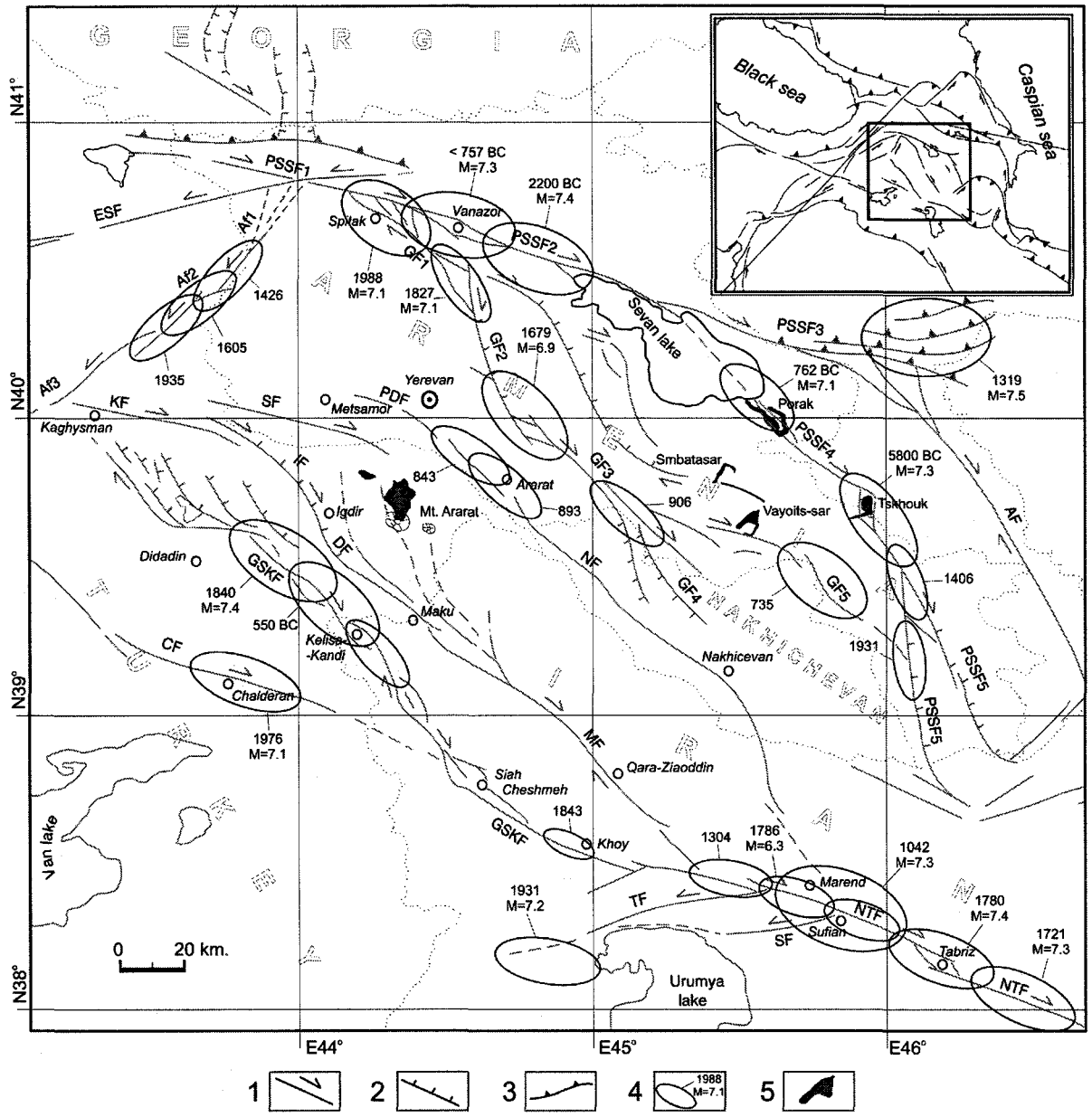

Fig. 1. Active faults of Armenia, Eastern Turkey and NW Iran. 1–strike–slips; 2–normal faults; 3–thrusts; 4–strong earthquake epicenters; 5–earthquake-triggered volcanic eruptions in the Holocene-historical time.

knowledge about this area reflects the fragmentation of studies between different countries of the region, while the transboundary character of main active faults means that cross-boundary cooperation is essential in natural hazard assessment studies in this region.

Recent manifestations of destructive seismic activity in the region include the 1976 ($M=7.1$) Chalderan,

1983 (M=6.8) Norman, 1988 (M=7.0) Spitak, and 1990 (M=7.3) Roudbar-Manjil earthquakes. Volcanic activity in the 20th century is limited to fumarole activity of Nemrout and Tondourek volcanoes (SE Turkey) and Sabalan volcano (NW Iran). Considering the regional rates of deformation, manifestations of seismic and volcanic activity recorded in the 20th century are not sufficient for a reliable hazard assessment. Moreover, historical and paleoseismicity information provide evidence for numerous strong earthquakes in the previous centuries (Stepanian, 1964; Ambraseys and Melville, 1982; Berberian, 1994, 1997; Guidoboni and Traina, 1995, 1996; Shebalin et al., 1997; Philip et al., 2001). Many of these earthquakes were accompanied by volcanic eruptions, large landslides, river migrations and other natural phenomena (Ambraseys and Melville, 1982; Karakhanian et al., 1997a,b, 2002; Philip and Karakhanian, 1999). Such secondary effects are important contributory elements in seismic hazard assessment. The greatest attention is given to soil effects enhancing seismic shaking, ground subsidence and liquefaction. However, earthquake-induced landslides may cause great destruction and large number of casualties, as demonstrated by the earthquakes of 1920 (M=8.5) in Gansu (China), 1948 (M=6.9) in Khait (Pamirs), 1970 (M=7.7) in Peru (Huascaran) (Keefer, 1994; Jibson et al., 1994; Jibson, 1996; Yeats et al., 1997). The effects of large landslides, volcanic eruptions and other secondary natural phenomena during strong earthquakes may add considerably to the damage and casualties and therefore can significantly alter the estimated seismic hazard level.

In this paper, we highlight the results of this integrated natural hazards approach with a detailed examination of three active fault test sites.

The three key sites are studied: (1) the Pambak-Sevan-Sunik fault (Armenia); (2) the Ararat Valley faults (the junction of borders of Armenia, Turkey, Iran and Azerbaijan); and (3) the Gailatu (Balikghel)-Siah Cheshmeh–Khoy and North Tabriz faults (the junction of borders of Iran and Turkey).

In tackling the cross-border nature of the active faults in this region, information on the faults has been compiled from researchers from Armenia, France, Russia, Iran and Turkey. This diverse group has used a wide range of investigation techniques to obtain its data: remote sensing, field and paleo-seismological research, radiometric (^{14}C) and archaeological dating methods and historical studies of ancient manuscripts and architectural monuments. For some sites, digital elevation models (DEM) and geographic information system (GIS) databases were created (using *Idrisi* and *Carta Linx* software). *Geo-Slope Slope/W* program has been used in slope stability calculations for large landslides.

2. Site 1: Pambak-Sevan-Sunik fault, Vanadzor depression

2.1. The Pambak-Sevan-Sunik fault

The Pambak-Sevan-Sunik fault (PSSF) has a total length of 490 km, stretching southeastwards from Lake Arpi (NW Armenia) to the valley of Arax, at the Armenia and Iran border (Fig. 1). Of all other active structures in Armenia, this fault has the greatest length and slip rates and is associated with the strongest earthquakes. Individual sites along the fault were studied in 1989–1990, 1993–1994 and 1997–2001 (Trifonov et al., 1990, 1994; Philip et al., 1992, 2001; Karakhanian et al., 1997a,b, 2002). These studies demonstrated that the PSSF consists of five large segments, each separated by overstep zones: the 90-km-long Arpi–Vanadzor segment (PSSF1), the 115-km-long Vanadzor–Artanish segment (PSSF2), the 120-km-long Artanish–Mrav segment (PSSF3); the 110-km-long Artanish–Tskhouk segment (PSSF4) and the 120-km–long Tskhouk–Zanghezour segment (PSSF5) (Fig. 1).

Along the entire length of the PSSF, there are signs of right-lateral strike–slip motion. The right-slip motions are often associated with a vertical component, mainly with a reverse-slip sense (Trifonov et al., 1994; Philip et al., 2001; Karakhanian et al., 1997b). The fault is characterized by strong historical earthquakes that occurred most notably in 915 ($M \sim 6.0$), 1407 ($M \sim 7.0$), and in 1187 and 1853 ($M \sim 6.0$) (Karakhanian, 1993; Shebalin et al., 1997). The largest historical earthquake ($M \sim 7.5$–7.7) on the PSSF was on the Artanish–Mrav segment in 1139. The 1139 earthquake was accompanied by the failure of large landslides and caused large-scale destruction and heavy casualties (Nikonov and Nikonova, 1986) The largest event for the 20th century occurred on the Tskhouk–Zanghezour segment in 1931 (M=6.5).

2.2. Vanadzor depression

Westwards from the junction of the Arpi–Vanadzor and Vanadzor–Artanish segments, the PSSF zone joins the Garni active fault (GF). At the site of junction, the Garni fault forms a horsetail splay structure of multiple young ruptures (Figs. 1 and 2). The westernmost of them is the surface rupture of the 1988 $M_s=7.1$ Spitak earthquake (SpF in Fig. 2). Areas between the Garni and Arpi–Vanadzor segments of the PSSF experience intense shortening, rotate in anticlockwise direction and are pushed out in the E–SE direction (Fig. 2) (Trifonov et al., 1994; Karakhanian et al., 1997b).

At the junction of the Arpi–Vanadzor and Vanadzor–Artanish segments, stepwise arranged fault segments of the PSSF zone create two jog-type structures that are occupied by the Vanadzor and Fioletovo depressions (Fig. 2).

The Fioletovo depression is 10 km long and up to 1.5 km wide. The depression is outlined by active faults with planes dipping outward from it and may be therefore characterized as a compressive structure. An elongated system of right-stepping en echelon pressure ridges aligns with the central axis of the Fioletovo depression and bears imprints of young scarps (Philip et al., 2001).

The fault of the northern flank of the Fioletovo depression continues on the southern flank of the Vanadzor depression (Fig. 2). The narrow neck linking the depressions near the village of Lermontovo (Fig. 2) bears traces of bending strain and of the overlap between the depressions along the right strike–slip separating them.

The Vanadzor depression is 16 km long and up to 3 km wide. It is bordered by numerous active faults with uplifted outer flanks. Young scarps inside the depression are formed along the en echelon faults (Figs. 2 and 3). Along one of such faults on the eastern depression flank, there is a clear right-lateral offset of large river thalwegs by 1400 m, with 25–30 m of vertical amplitude, and smaller drainage courses by 450 m (Figs. 4 and 5).

Cumulative horizontal displacements recorded along the Arpi–Vanadzor segment (points 1 and 2 in Fig. 2) range from 1.8 (young tributaries) to 2 km (large valleys), and the vertical displacements are 10–15 m (Trifonov et al., 1990; Rebai et al., 1993). At the site of Vanadzor and Fioletovo depressions, horizontal displacement amplitudes decrease to 1.4 km, while the vertical ones increase to 30–60 m.

Horizontal slip rate estimates are 3–4 mm/year for the Arpi–Vanadzor segment (point 1 in Fig. 2) (Trifonov et al., 1990) and 2.8 mm/year for the Vanadzor–Artanish segment (point 3 in Fig. 2) (Philip et al., 2001). The slip rates estimated from the Khonarassar volcano displacement on the Artanish–Tskhouk segment have a much greater discrepancy, ranging between 3–4 (Trifonov et al., 1994) and 0.53 ± 0.04 mm/year (Philip et al., 2001). The disparity in slip rates between the Arpi–Vanadzor and Vanadzor–Artanish segments may be explained by strain accumulation within the Vanadzor and Fioletovo depressions.

2.3. Hazard assessment

Although there are many signs of young tectonic activity, no records of strong historical seismicity are available for the Vanadzor depression and for the adjacent PSSF segments. The only historical earthquake was in 1915, and this had the magnitude of $M=5.3$. However, the absence of large historical architecture monuments in this region despite its great cultural importance in the period of 12th–15th centuries AD suggests that the historical seismicity database is, possibly, incomplete. Ruins of a church dated back to the 12th–15th centuries AD, found to the northwest of the village of Meghrout, have signs of reconstruction in the 13th–14th centuries AD. The foundation of this church is strongly damaged, and stone steles (so-called khachkars) near the church are thrown out of their basements, which points to a possible strong earthquake between the 12th and 13th centuries AD. A part of crumbled man-made grottos in a cave monastery of the 11th–13th centuries AD, west of the city of Spitak can also bear witness to a seismic impact. Historical evidence indicate that an earthquake of $M=6.5$–7.0 in 1827 could occur on the GF2 segment of the Garni fault (Trifonov et al., 1994).

The seismic hazard assessment conducted before 1988 based on historical seismicity data provided a 7–8 intensity estimate (~ 0.2 g) for the region encompassing the cities of Spitak and Vanadzor (Kondorskaya and Shebalin, 1980). The Spitak earthquake of

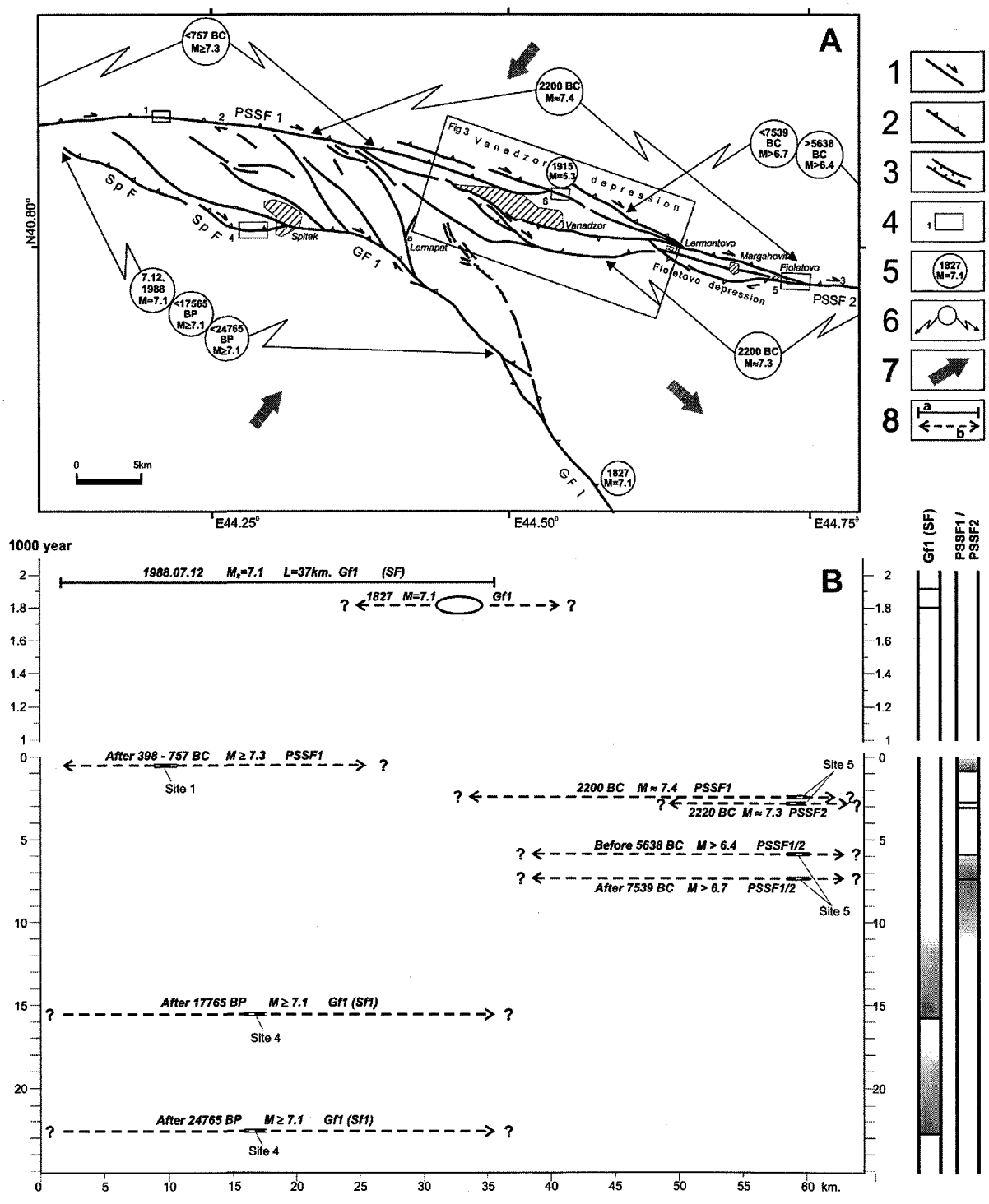
A
<757 BC M≥7.3
2200 BC M≈7.4
PSSF 1
Fig 3
Vanadzor depression
1915 M=5.3
<7539 BC M>6.7
>5638 BC M>6.4
SpF
SpF 4
Spitak
GF 1
Lermontovo
Margahovit
Fioletovo
Fioletovo depression
PSSF 2
7.12. 1988 M=7.1
<17565 BP M≥7.1
<24765 BP M≥7.1
2200 BC M≈7.3
1827 M=7.1
N40.80°
0 5km
E44.25°
E44.50°
E44.75°
1
2
3
4
5
6
7
8
B
1000 year
1988.07.12 Ms=7.1 L=37km. Gf1 (SF)
1827 M=7.1 Gf1
After 398 - 757 BC M ≥ 7.3 PSSF1
Site 1
2200 BC M ≈ 7.4 PSSF1
2220 BC M ≈ 7.3 PSSF2
Site 5
Before 5638 BC M > 6.4 PSSF1/2
After 7539 BC M > 6.7 PSSF1/2
Site 5
After 17765 BP M ≥ 7.1 Gf1 (Sf1)
Site 4
After 24765 BP M ≥ 7.1 Gf1 (Sf1)
Site 4
0 5 10 15 20 25 30 35 40 45 50 55 60 km.
Gf1 (SF)
PSSF1 / PSSF2

1988 (M_s = 7.1) proved the hazard was underestimated. The earthquake produced a 32-km-long surface rupture (SpF) on the western branch of the horsetail splay structure, linking the GF and PSSF zones (Fig. 2), and caused severe destruction in the cities of Spitak, Vanadzor and Giumri, as well as in numerous villages, killing about 27,000 people. The 1988 Spitak earthquake demonstrated that duration of the historical seismicity record was not sufficient to provide a reliable seismic hazard estimate.

Our paleoseismological studies in 1989–2001 revealed signs of several prehistorical surface ruptures generated by $M \sim 7.0$–7.4 earthquakes in the PSSF and GF zones (Philip et al., 1992, 2001; Avagyan, 2001). Ages of these events estimated by ^{14}C method are presented in Table 1. These ^{14}C estimates were calibrated against the *Radiocarbon calibration program rev.4.3* of Stuiver and Reimer (1993). Unless otherwise specified, we cite calibrated age estimates in years BP (1σ). Archeological dating of artifacts discovered in many of the trenches also helped to define the age of the paleo-earthquakes (Philip et al., 2001; Avagyan, 2001). In this work, we give ages in years BC or AD if these were estimated, or better constrained by archaeological dating. Vertical and oblique displacements recorded in the trenches were used to calculate the magnitudes of paleo-events by empirical relationships (Wells and Coppersmith, 1994). Whenever impossible to estimate the length of paleo-rupture, magnitudes were derived from the seismic moment (Hanks, 1979). Table 2 presents ages of displacements in paleo-events measured by ^{14}C and archaeological methods, and magnitudes calculated for the PSSF and GF segments.

Paleoseismological studies in the rupture area of the 1988 Spitak earthquake (site 4 in Fig. 2) revealed one $M \sim 7.1$ event that occurred after cal. (calibrated) 21274–20519 years BP (1σ) (17565 ± 170) and a second probable event that occurred after 24765 ± 770 years BP (Tables 1 and 2, Philip et al., 1992), although it is not possible to calibrate this latter date since it is beyond the time span of the *Radiocarbon calibration program rev.4.3* (Stuiver and Reimer, 1993).

Paleoseismological studies on the east flank of the Fioletovo depression (point 5 in Fig. 2) revealed surface ruptures from two nearby seismic events that occurred about 2200 BC (Tables 1 and 2). One of those events with a magnitude of $M \sim 7.4$ occurred on the Arpi–Vanadzor segment (PSSF1) and the other with $M \sim 7.3$ on the Vanadzor-Tsovagiugh segment (PSSF2). The estimated age of the second paleo-event ($M \sim 7.3$) recorded for the PSSF1 is cal. 2707–2348 years BP (1σ). On the PSSF2 segment, we recorded signs of other three events with estimated magnitudes of >6.7, >6.4 and ~ 7.3: one of them is predated, and the other postdated by cal. 9489–7588 years BP (1σ), while the third event is postdated by 21705 ± 240 years BP (again, this date must remain uncalibrated).

Paleoseismological studies indicate that the Pambak-Sevan-Sunik and Garni faults, whilst characterized by relatively low slip rates (4–1.5 mm/year) and long intervals of earthquake recurrence (2000–10,000 years and more), can nevertheless generate M = 7.2–7.4 earthquakes (Table 3).

Therefore, the PSSF1 and PSSF2 segments, with estimated $M_{max} \sim 7.3$–7.4 and earthquake recurrence intervals from 2000 to 4000 years, and the GF1 segment, with estimated $M_{max} \sim 7.1$ and a recurrence interval of more than 10,000 years, pose the greatest hazard for the region of Vanadzor and Fioletovo depressions (Table 3). An important fact to consider is that the time elapsed after the last strong earthquakes took place on the PSSF1 and PSSF2 segments approaches the respective estimate of earthquake recurrence interval (PSSF1) and even exceeds it (PSSF2).

The city of Vanadzor occupies the western flank and the centre of the Vanadzor depression; the depression also accommodates the large villages of Meghrout, Shahoumian and Darpas. According to the effective Earthquake Engineering Code of the

Fig. 2. (A) Active faults in the region of the Vanadzor and Fioletovo depressions: 1–strike–slip faults; 2–reverse faults and thrusts; 3–normal faults; 4–locations of fault slip rate measurements and palaeoseismological work; 5–macroseismic epicenters of historical earthquakes; 6–surface ruptures from strong earthquakes; 7–regional stress field directions; 8a–documented surface rupture; 8b–surface rupture inferred by paleoseismological studies. (B) Space and time distribution diagram for earthquakes that produced surface ruptures on PSSF1, PSSF2 and GF1.

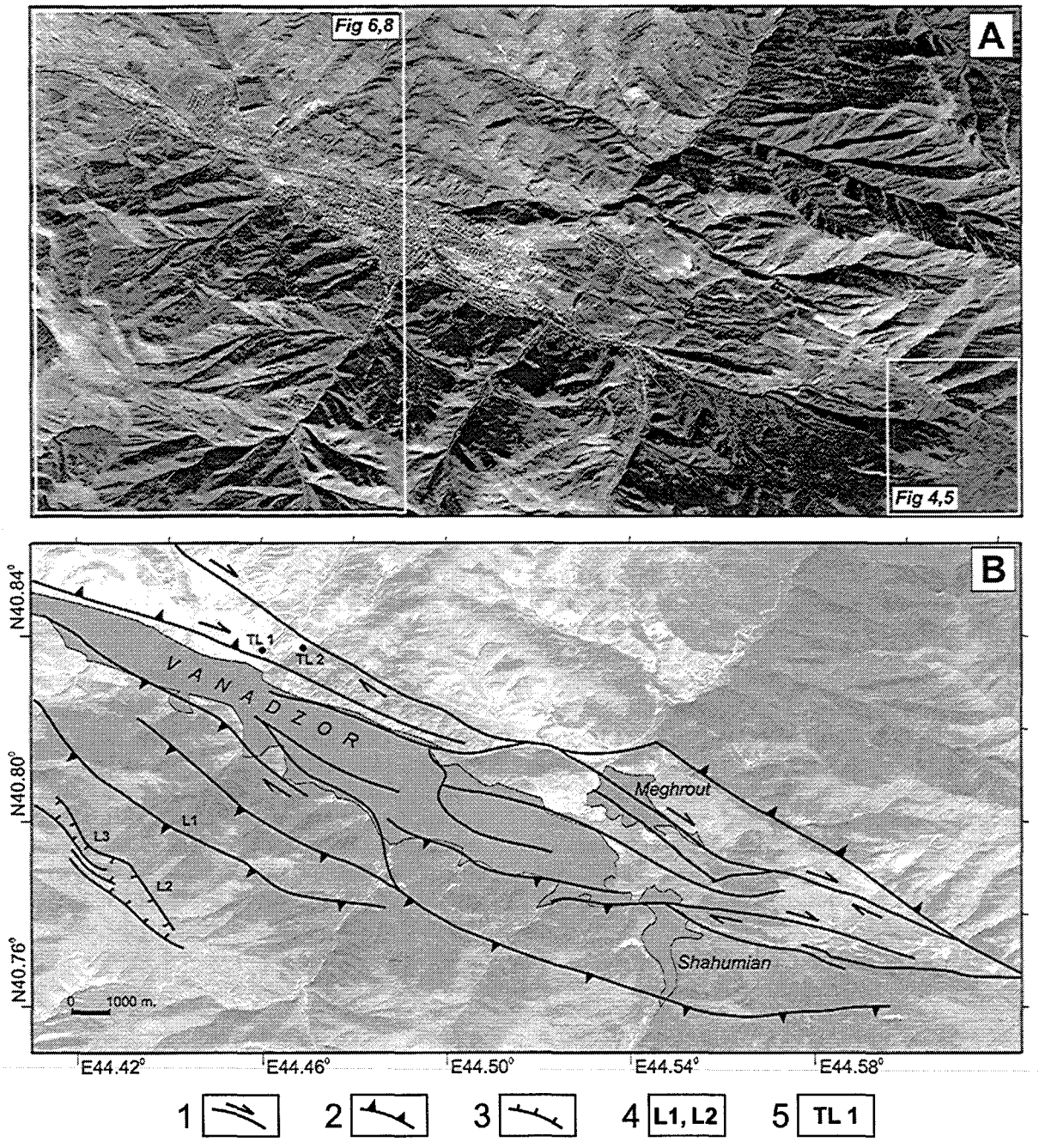

Fig. 3. Active faults in the Vanadzor depression: (A) Landsat 7ETM+satellite image; (B) interpretation. 1–strike–slips; 2–normal faults; 3–reverse faults; 4–landslides; 5–populated areas.

Republic of Armenia (Khachiyan, 1998), the area has a deterministic estimate of maximum PGA value of 0.4 *g*. In 1999, several agencies revised the estimation of PGA values for the western part of the city of Vanadzor, resulting in a deterministic estimate of 0.6*g* and probabilistic estimates of 0.34*g*

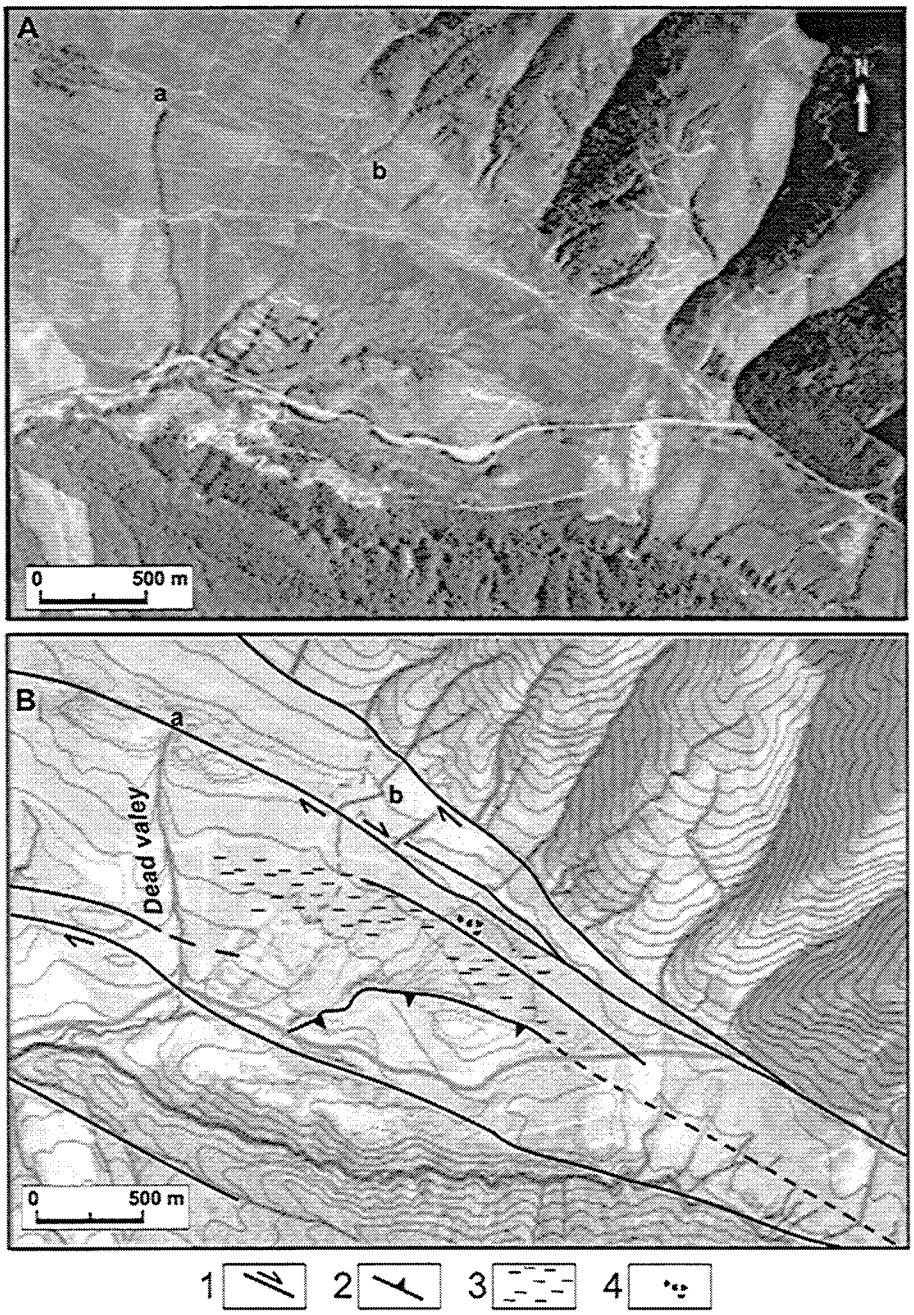

Fig. 4. East part of the Vanadzor depression: (A) air photo, (B) interpretation: 1–strike–slips; 2–reverse faults; 3–marshy areas; 4–young alluvial fans; A–B–river valley offset amplitude.

(for 30 years), 0.38*g* (for 100 years) and 0.5*g* (for 500 years) with 90% probability (Seismic Hazard Assessment, 1999).

The city of Vanadzor and surrounding villages have a total population of 183,000. A large chemical plant (point 1 in Fig. 6), synthetic fiber factory and

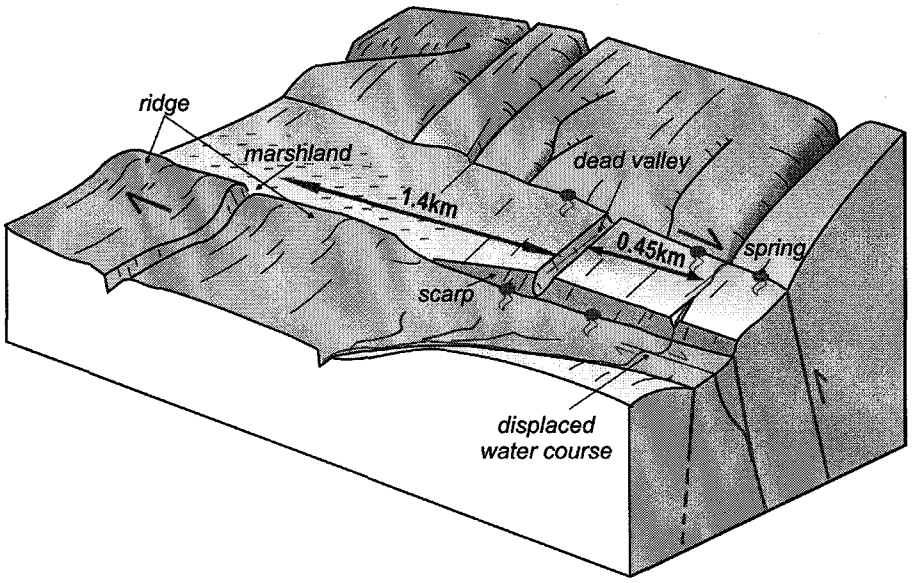

Fig. 5. 3-D model of the eastern flank of the Vanadzor depression.

thermal power plant (TPP) (points 2 and 3 in Fig. 6) are all located in the western part of the city.

Widespread large landslides, some of which have recently displayed creep activity, are an important natural hazard for the city of Vanadzor. Three large

Table 1
Summary of sample locations, material and age estimates obtained by radiocarbon dating

Site	Trenches	Sample	^{14}C-age estimate (years BP)	Calibrated age BP (1σ)	Calendar BC ages (1σ)	Materials	Laboratory
1	Gogaran	2a	2402 ± 63	2707 (2357) 2348	757 (408) 398	paleosoil	UPS
6	Meghrout	3	21,705 ± 240	–	–	carbonate	UPS
6	Meghrout	4	26,000 ± 800	–	–	paleosoil	RGI
6	Meghrout	6	132 ± 51	278 (140) 0*	1672 (1810) 1951 (AD)	soil	UPS
5	Fioletovo I	1bA	7600 ± 860	9489 (8390) 7588	7539 (6440) 5638	paleosoil	UPS
5	Fioletovo III	4a	5930 ± 330	7228 (6745) 6354	5278 (4795) 4404	charcoal	UPS
5	Fioletovo III	3a	5410 ± 420	6660 (6243) 5722	4710 (4293) 3772	charcoal	UPS
5	Fioletovo III	3a	5270 ± 740	6854 (5992) 5092	4904 (4042) 3142	charcoal	UPS
5	Fioletovo III	2A	5030 ± 170	5932 (5832) 5597	3982 (3882) 3647	paleosoil	RGI
5	Fioletovo III	2A	4885 ± 1225	6986 (5604) 3934	5036 (3654) 1984	charcoal	UPS
5	Fioletovo III	3b	4735 ± 470	5933 (5553) 4835	3983 (3603) 2885	charcoal	UPS
5	Fioletovo III	3a	4340 ± 70	5028 (4866) 4837	3078 (2916) 2887	charcoal	UPS
5	Fioletovo III	5A; 4bA	2230 ± 60	2337 (2207) 2150	387 (257) 200	paleosoil	UPS
3	Semionovka IV	2A	3799 ± 66	4283 (4174) 4089	2333 (2224) 2139	paleosoil	UPS
3	Semionovka IV	2AB	2490 ± 120	2749 (2585) 2353	799 (636) 403	soil	RGI
	Tsoursar	3A	6640 ± 90	7605 (7536) 7431	5655 (5587) 5481	paleosoil	UPS
4	Spitak III	2b	24,765 ± 770	–	–	organic	UPS
4	Spitak III	3	19,960 ± 225	[24,111] (23,648) 23,196	[22,161] (21,699) 21,246	turf	UPS
4	Spitak III	3	17,565 ± 170	21,274 (20,892) 20,519	19,324 (18,943) 18,569	turf	UPS

0* represents a *negative* age in years BP (Stuiver and Reimer, 1993).
[ ] calibrated with an uncertain region or a linear extension to the calibration curve (Stuiver and Reimer, 1993).

Table 2
Mean values of earthquake recurrence intervals, magnitudes, and surface rupture offsets

Fault segment	Age of displacement calculated by ^{14}C and archeological data					Vertical offset (m)	Oblique offset (m)	Mw by Wells and Coppersmith (1994)
	Event	Predate (years BP)	Postdate (years BP)	Calculated average age				
				BP	Calibrated age, BC/AD			
PSSF1	1	2402 ± 63	–	<2707 (2357) 2348	<757 (408) 398	>1.20	>2.4 (ad)	>7.3
	2	4340 ± 70	2230 ± 60	–	2200 ± 200*	3.6	7.2 (md)	7.4
PSSF2	1	3799 ± 66	2490 ± 120	–	2200 ± 200*	2.3	4.6 (md)	7.3
	2	7600 ± 860	–	<9489 (8390) 7588	<7539 (6440) 5638	>0.4	>0.8 (md)	>6.7
	3	–	7600 ± 860	>9489 (8390) 7588	>7539 (6440) 5638	>0.18	>0.36 (md)	>6.4
	3	21,705 ± 240	132 ± 51	–	–	2.4	4.8 (md)	7.3
PSSF3	1	6640 ± 90	–	–	782–773*	≥1.1–1.8	2.4 (ad)	≥7.3
PSSF4	1	–	5337 ± 68, 5000 ± 700	10,500 ± 1600 OSL	–	2.60	>4.0 (md)	>7.2
GF1	1	24,765 ± 770	17,565 ± 170	–	–	≥2.15	≥2.9 (md)	≥7.1
	2	17,565 ± 170	7.12 1988 AD	<21,274 (20,892) 20,519	<19,324 (18,943) 18,569	≥2.15	≥2.9 (md)	≥7.1
	3	–	–		7.12 1988 AD	1.8	2.5 (md)	7.1

* by archaeological data.
md–maximum surface displacement.
ad–average surface displacement.

Table 3
Seismotectonic characteristics of segments of the Pambak-Sevan-Sunik (PSSF) and the Garni (GF) active faults

Fault segments		PSSF1	PSSF2	PSSF4	PSSF5	GF1
Max coseismic offset[a] vertical/oblique* (m)		3.6/7.2	2.40/4.8	1.10/2.40	2.60/4	1.80/≥2.15
Long-term horizontal displacement[b] (m)		2000 ± 250	1850 ± 50	750 ± 50	–	300 ± 50
Long-term slip rate[c] (mm/year)	horizontal	3–4 ± 0.5	2.22 ± 0.95	1.3–1.5 ± 0.5	1.3 ± 0.5	3 ± 0.5
	vertical	0.4–0.5 ± 0.5	1.28 ± 0.55	0.2–0.3 ± 0.5	–	0.3–0.4 ± 0.5
Short-term slip rate[d] (mm/year)	horizontal	2.73	2.7	0.64 ± 0.07	>0.39 ± 0.04	–
	vertical	–	–	0.28 ± 0.03	>0.33 ± 0.03	–
Estimated M_{max}	Hist.[e] (Ms)	5.0	5.5	6.5	6.5	7.1
	TL[f] (Ms)	6.7	6.7	6.5	6.7	6.6
	D[g] (Mw)	7.4	7.3	7.3	>7.2	≥7.1
Recurrence time M>7.0 (years)	Geological method[h]	1622 ± 179	>4388 ± 950	4675 ± 207	≤10,500 ± 1600	<20,934 ± 377
	Direct method[h]	2240 ± 640	3970 ± 1698	3444 ± 637	–	–
Elapsed time (years)		2579 ± 179	4202 ± 200	2779 ± 4.5	≤10,500 ± 1600	14

[a] by paleoseismological and archeoseismological data.
[b] by morphostructure data.
[c] by displacements of morphological elements.
[d] by offsets of man-made structures and stratigraphic units.
[e] by McCalpin and Nelson, 1996.
[f] by Slemmons, 1982.
[g] Wells and Coppersmith, 1994.
[h] by Working Group, 1988.

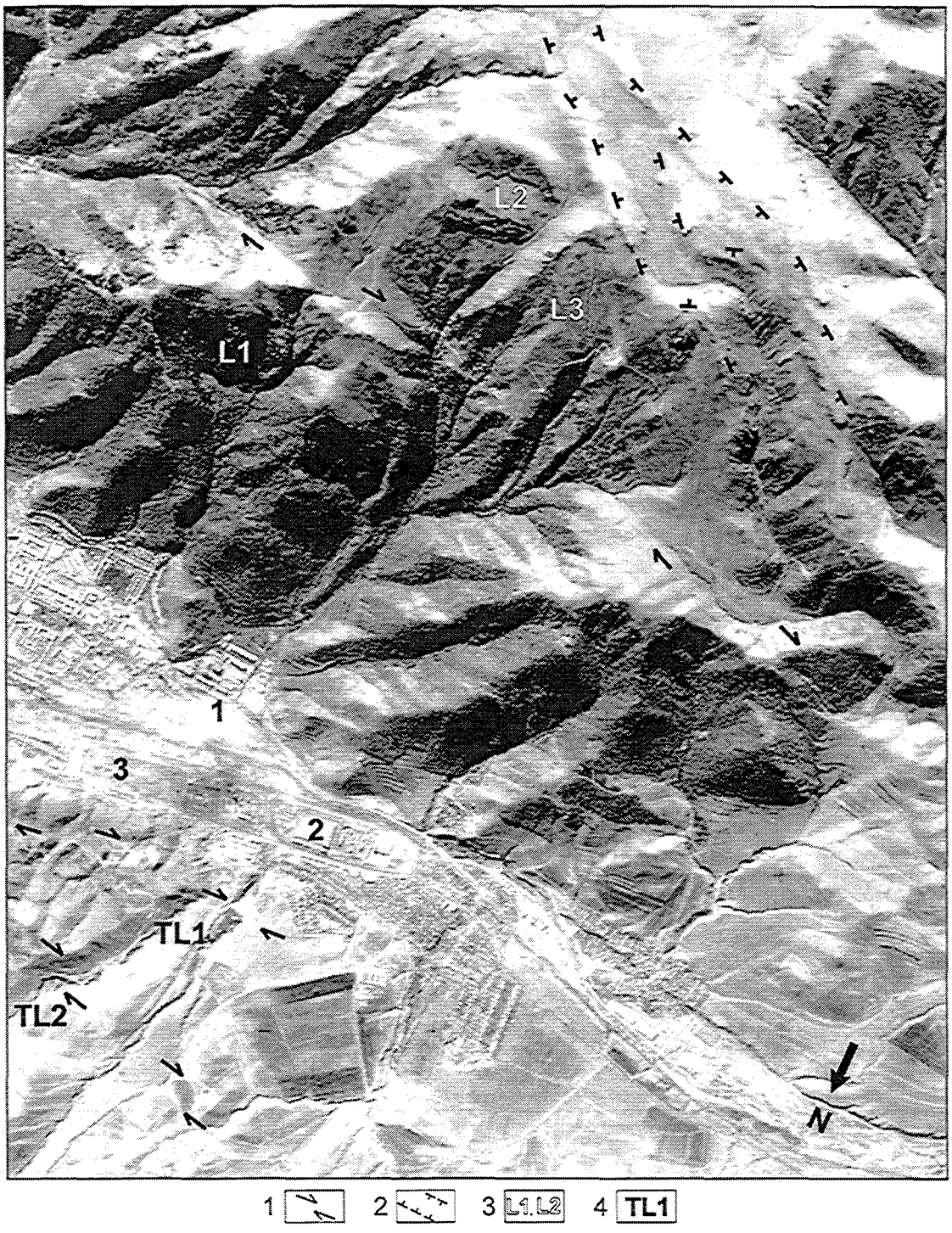

Fig. 6. Air photo of the west part of the Vanadzor depression: 1–strike–slips; 2–normal faults; 3–L1, L2 and L3 landslides; 4–TL1 and TL2, toxic waste repositories of the Vanadzor chemical plant; point 1–Vanadzor chemical plant; point 2–synthetic fiber factory; point 3–TPP.

Table 4
Volumes and locations of the landslides and toxic waste repositories in the city of Vanadzor

Landslides/waste repositories	Volume of landslide/ waste repository (in million m^3)	Altitude drop between the landslide/waste repository and the city (in m)	Distance from the city to the landslide/waste repository crest (in m)	Average slope gradient between the landslide/ waste repository and the city
Landslide L1	80	640	850	19
Landslide L2	160	1000	2700	14
Waste repository TL1	3	70	300	7
Waste repository TL2	4	200	1100	7

landslides (L1, L2 and L3 in Fig. 6; Table 4) are directly upslope from the city of Vanadzor and its chemical plant, on the southwestern flank of the Vanadzor depression.

Detachment scarps of all three landslides have formed directly in the zone of the PSSF2 segment that flanks the Vanadzor depression in the south (Fig. 6). Precipitation in the Vanadzor depression is particularly high and contributes to more intensive landsliding. Mass deforestation on L1, L2 and L3 landslide slopes during the last 10 years has been an important factor in increasing the hazard.

On the NW side of the Vanadzor depression, there are two chemical plant waste repositories (TL1 and TL2) upslope of the synthetic fiber factory and TPP (Figs. 6 and 7; Table 4). Repository TL1 is filled with melamine production wastes, while repository TL2 contains high toxic melamine and carbide wastes that in humid conditions can absorb water rapidly (i.e., they are hygroscopic) and transform into a flow of liquid inviscid pulp. The wastes in TL2 are in semi-liquid and liquid condition.

Both dams of the waste repositories were built in 1972 directly on active fault zones. The dams are earthfill embankments in deep ravines just at the site of abrupt right-lateral offset of the ravines by the slip along the PSSF segments, bordering northern flanks of the Vanadzor depression (Figs. 3, 6 and 8). The

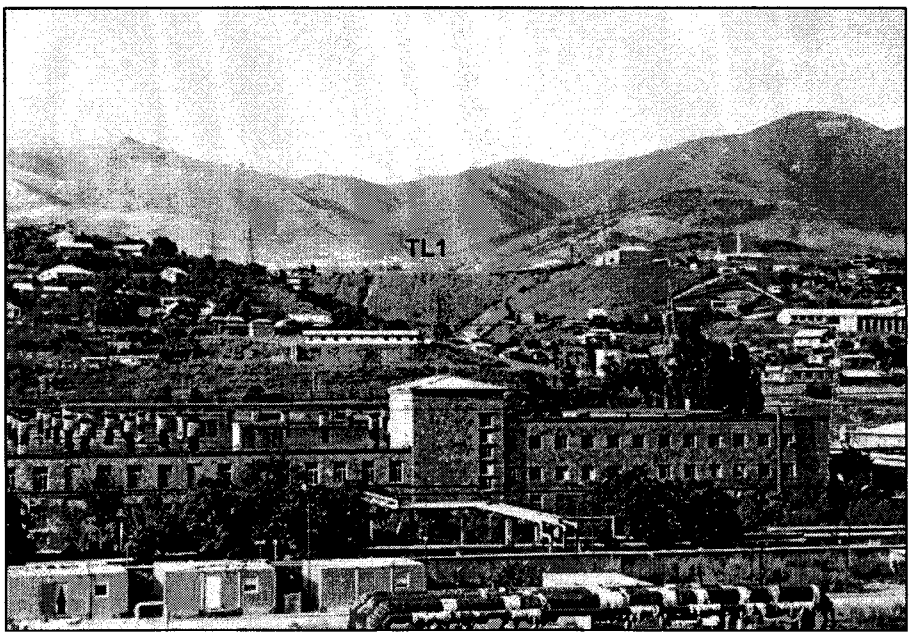

Fig. 7. The dam of TL1 repository of toxic wastes from the Vanadzor chemical plant.

Table 4
Volumes and locations of the landslides and toxic waste repositories in the city of Vanadzor

Landslides/waste repositories	Volume of landslide/ waste repository (in million m^3)	Altitude drop between the landslide/waste repository and the city (in m)	Distance from the city to the landslide/waste repository crest (in m)	Average slope gradient between the landslide/ waste repository and the city
Landslide L1	80	640	850	19
Landslide L2	160	1000	2700	14
Waste repository TL1	3	70	300	7
Waste repository TL2	4	200	1100	7

landslides (L1, L2 and L3 in Fig. 6; Table 4) are directly upslope from the city of Vanadzor and its chemical plant, on the southwestern flank of the Vanadzor depression.

Detachment scarps of all three landslides have formed directly in the zone of the PSSF2 segment that flanks the Vanadzor depression in the south (Fig. 6). Precipitation in the Vanadzor depression is particularly high and contributes to more intensive landsliding. Mass deforestation on L1, L2 and L3 landslide slopes during the last 10 years has been an important factor in increasing the hazard.

On the NW side of the Vanadzor depression, there are two chemical plant waste repositories (TL1 and TL2) upslope of the synthetic fiber factory and TPP (Figs. 6 and 7; Table 4). Repository TL1 is filled with melamine production wastes, while repository TL2 contains high toxic melamine and carbide wastes that in humid conditions can absorb water rapidly (i.e., they are hygroscopic) and transform into a flow of liquid inviscid pulp. The wastes in TL2 are in semi-liquid and liquid condition.

Both dams of the waste repositories were built in 1972 directly on active fault zones. The dams are earthfill embankments in deep ravines just at the site of abrupt right-lateral offset of the ravines by the slip along the PSSF segments, bordering northern flanks of the Vanadzor depression (Figs. 3, 6 and 8). The

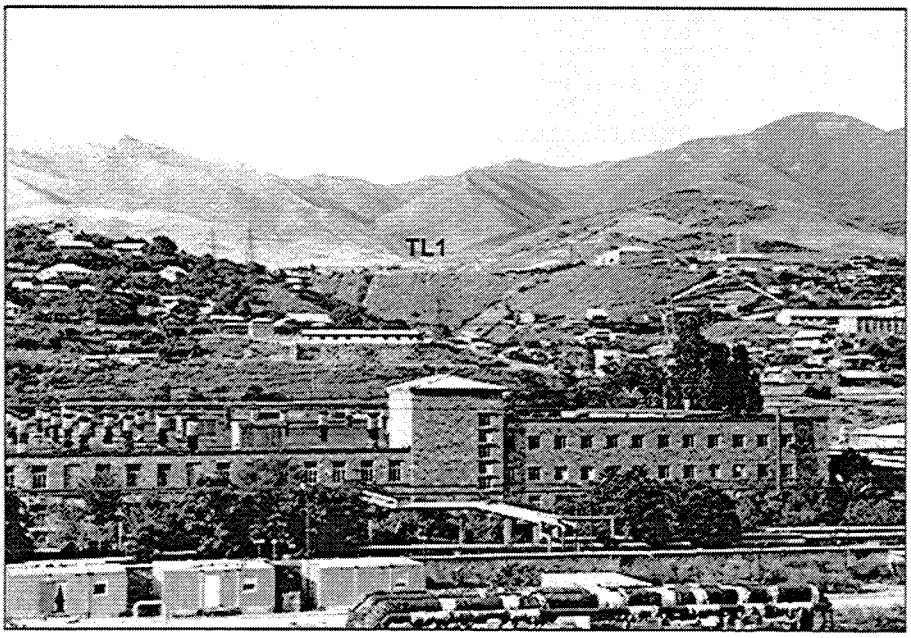

Fig. 7. The dam of TL1 repository of toxic wastes from the Vanadzor chemical plant.

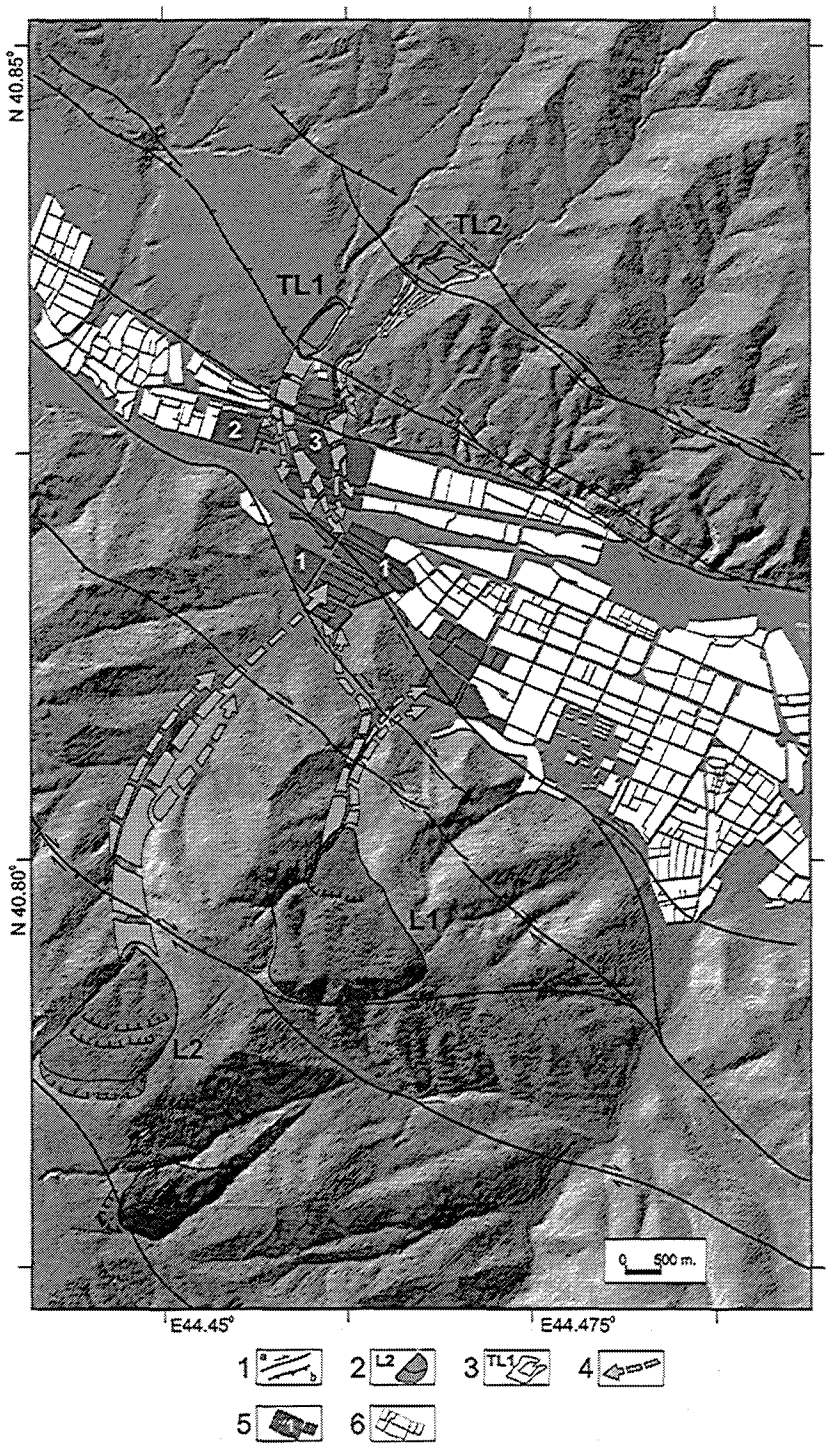
N 40.85°
N 40.80°
E44.45°
E44.475°
TL1
TL2
L1
L2
1
2
3
0 500 m.
1 2 3 4
5 6

Table 5
Stability characteristics for landslide slopes and scarps of toxic waste repository dams in the city of Vanadzor

Landslides/ waste repositories	Estimated landslide mass displacement[a] (cm) (Birbrayer and Krasenkov, 1973)		Estimated displacement of landslide/repository mass with a coseismic slip on the fault (cm) (Wells and Coppersmith, 1994)		Threshold PGA value (fractions of g) that destabilizes the dam[b]	Destructive mass travel in case of catastrophic failure of landslides/repository dams (m) (Davies, 1982)
	PGA=0.35	PGA=0.55	PGA=0.35	PGA=0.55		
Landslide L1	120	226	60	350		4300
Landslide L2	122	229	60	350		5500
Waste repository TL1			60	350	0.25	1300
Waste repository TL2			60	350	0.1	1600

[a] The magnitudes and rates of landslide body displacement were derived solving a plane problem on the degree of rotation of ground slope failure prism for a circular-cylinder failure surface under the seismic impact of design accelerogram (Birbrayer and Krasenkov, 1973).

[b] Dams of waste repositories TL1 and TL2 are built with pebble and gravel soils characterized by the following physical and mechanical parameters: internal friction angle of 35°; cohesion of 0 mPa; 1.9 t/m^3 volumetric rock weight under natural humidity conditions; and 1.98 t/m^3 volumetric weight of water-saturated rocks. The core task was to estimate the acceleration value that would bring the dam slope to an equilibrium limit state. The problem was solved through selection of an acceleration value to determine Safety Factor verging to 1.

eastern bank of the ravine under the TL1 headwall is actively sliding. Both of the dams were weakened by the 1988 Spitak earthquake and damaged in the following years.

To assess the hazard for the city of Vanadzor, seismic acceleration values capable to destabilize dam slopes and cause earthquake-triggered displacement of the landslides were estimated.

The calculations show that landslides L1 and L2 will start to move intensively under the impact of a 0.3g (M ~ 6.3) earthquake and will slip 120–122 cm downslope at a speed of ~ 50 cm/s. A 0.55g impact (M7.3) can cause dislocation for 226–229 cm at a speed of ~ 90 cm/s (Table 5). In 6 s (duration of the design earthquake), the landslides will gain fast and destructive downslope motion under seismic and gravitational forces and will travel a considerable distance.

Calculation of the marginal seismic acceleration causing destruction of TL1 and TL2 dams was again based on the D-17-85/BH?ÈÃ and SNIP II-7-81 code, and *Geo-Slope Slope/W* software (Karakhanian et al., 2000). The calculations showed that TL1 dam failure would initiate at acceleration values higher than 0.25g, while destruction of the TL2 dam would start at acceleration values higher than 0.1g (Table 5).

In addition to considering the effect of active faults on landslide scarps and dam bodies, we can estimate expected coseismic displacement on these faults by the method proposed by Wells and Coppersmith (1994) assuming that fault slip will involve a similar amplitude offset of the whole mass of the landslides and dams. Calculations by empirical fault relations of Wells and Coppersmith (1994) for faults of reverse and strike–slip kinematics derive coseismic slip of 60 cm for an $M=6.3$ earthquake and 350 cm for an $M=7.3$ earthquake. The results indicate that an $M=6.3$ earthquake may cause failure of landslides L1 and L2 and dams TL1 and TL2 (Table 5).

Using the formula of Davies (1982), it is possible to calculate probable transit distance of destruction masses in case of failure of landslides L1, L2 and L3 and destruction of TL1 and TL2 dams (Table 5). To calculate the potential affected area, digital elevation models were built at the scales of 1:25,000 and 1:5000, and a GIS-format database was created (Fig. 8).

Fig. 8. GIS hazard data for the west part of the Vanadzor depression. 1–Active faults (a–strike–slips, b–reverse faults); 2–landslides L1 and L2; 3–toxic waste repositories TL1, TL2 of the Vanadzor chemical plant; 4–transit of the landslide masses and toxic waste mass from the repositories in case the latter are destroyed; 5–industrial facilities (1–Vanadzor chemical plant, 2–synthetic fiber factory; 3–TPP) and city districts in the affected area; 6–city districts beyond the affected area.

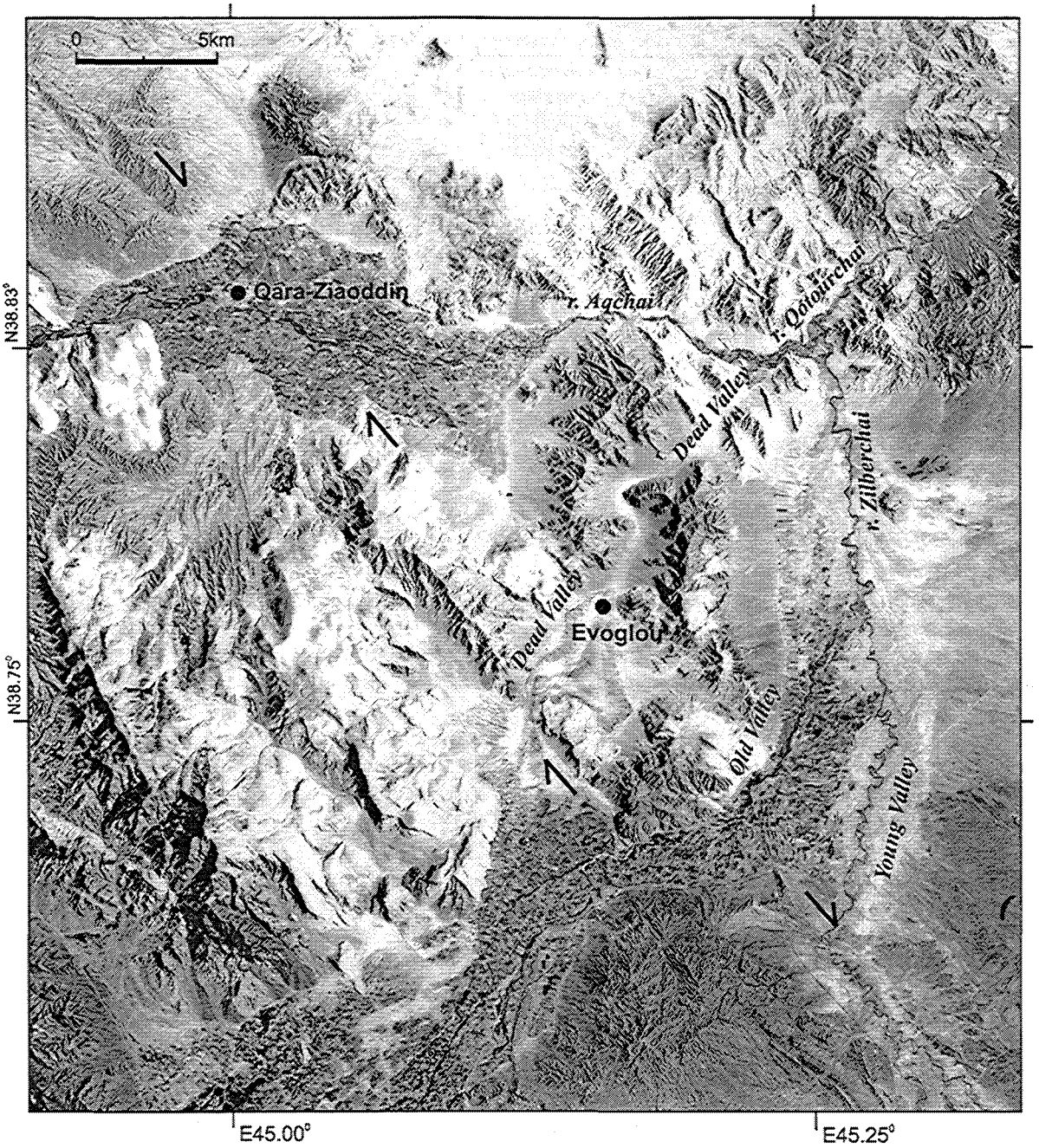

Fig. 9. SPOT satellite image of the right-lateral displacements of the Qotourchai River and its tributaries—Aqchai, Qotourchai and Zilberchai—along the Maku fault. Tectonic dam basins of Evoglou and Qara-Ziaoddin (see Fig. 1, Qara-Ziaoddin).

If a 0.3g acceleration (M=6.3) earthquake produces a surface rupture on the PSSF1 and PSSF2 segments, bordering the Vanadzor depression, all three landslides may activate and slide down, while the dams of toxic waste repositories will be expected to fail at even lower acceleration values (0.1–0.25g).

Traveling down the valleys, the failure masses can reach the city of Vanadzor and devastate considerable areas in the west part of the city (Fig. 9).

Based on analysis of the GIS database, the risk for the city of Vanadzor with the population of 183,000 in case of such a landslide disaster, triggered by a 0.3*g* acceleration earthquake and accompanied by toxic waste outbursts, is estimated as fatalities up to 10–20% of the population, the widespread devastation of the southwestern part of the city, and the total destruction of the chemical plant, synthetic fiber factory and the TPP. Considering that the seismic hazard estimate is 90% probability of a 0.34*g* event within 30 years (Seismic Hazard Assessment, 1999), the above may be assumed as realistic risk assessment for such a scenario. The economic cost of material damage at this level of risk is difficult to estimate, but the casualties may reach 10,000–20,000 people, i.e., numbers comparable to the 1988 Spitak earthquake (27,000 deaths).

In summary, integrating the natural and man-made hazards (earthquakes, landslides, dams and toxic wastes) in active fault zones bordering the Vanadzor depression lowers from 0.4*g* (Khachiyan, 1998) to 0.2–0.3*g* the level of seismic hazard (maximum permissible level, MPL) that may cause considerable destruction and human casualties.

3. Site 2: Ararat depression

The Ararat depression is at the junction of state borders of Armenia, Turkey, Iran and Azerbaijan. There remains much not known about the structural position of the Ararat depression. Dewey et al. (1986) point out that it is a complex pull-apart graben on a wide zone of right-lateral transcurrent motion. In contrast, Yilmaz et al. (1998) consider that the Ararat depression is a left-lateral pull-apart basin, developed along a zone of extension between two en echelon segments of the left-lateral strike–slip fault system.

To analyze the structural position of the Ararat depression and assess the associated natural hazard, we studied remote sensing data, historical and archaeological sources and conducted fieldwork in the territory of Turkey (1993), Iran (1996) and Armenia (1997–2000).

The Ararat depression is a large structure of pull-apart basin type elongated in NW direction, with a width of 20–35 km. The northeastern flank of the Ararat pull-apart is represented by the zone of Sardarapat–Nakhichevan active faults. The Dogubayazit and Maku active faults form its southwestern flank (Fig. 1); individual segments of these faults are described by Berberian (1976, 1981, 1997), and Barka and Kadinsky-Cade (1988). The Gailatu–Siah Cheshmeh–Khoy fault is located 10–20 km southeast of the Maku and Dogubayazit faults (Berberian, 1976, 1997; Karakhanian et al., 1996).

3.1. The Sardarapat–Nakhichevan fault system

This fault system consists of four en echelon segments: Kagyzman (KF), Sardarapat (SF), Parackar–Dvin (PDF) and Nakhichevan (NF) (Fig. 1). The segments form a left-stepping system that trends from the city of Kagyzman (Turkey) into Armenia, where it passes south of the city of Yerevan and north of the villages of Dvin and Artashat. In the southwest, the fault zone continues into Azerbaijan and Iran. In the region of Nakhichevan (Azerbaijan), the zone is aligned NW–SE and possibly trends toward the city of Marand (Iran).

The 70–75-km-long Sardarapat segment is the most active, with uplift of up to 40–70 m above the Ararat depression surface. The Sardarapat uplift forms ranges of hills composed of the Quaternary alluvial and deluvial deposits and basalts. Graben-shaped depressions formed along the central depression axis, the sides of which are defined by subvertical ruptures. The arrangement appears consistent with a palm tree-type flower structure formed over a strike–slip zone. At the eastern end of the fault, an ancient irrigation canal is uplifted along the fault and is 25 m higher than the depression it had been laid in. ^{14}C dating of a charcoal sample taken from the canal deposits provides the age of cal. 3832–3470 years BP (1σ) (3400 ± 140 years BP (Geological Institute of Russia)). Archeological data support the validity of this estimate and suggest a vertical slip rate of about 0.7 mm/year on the Sardarapat fault; it has not been possible to estimate the horizontal slip rate.

3.2. Maku and Dogubayazit faults

The analysis of satellite images indicates that the Maku fault (MF) passes along the southwestern flank

of the Ararat pull-apart (Fig. 1). Individual segments of this fault are described by Berberian (1976, 1981, 1997). We succeeded in tracing the fault from the west of the city of Marand to the populated areas of Evoglou, Qara-Ziaoddin, Shahabad in Iran and farther to the northwest, into Turkey, where it joins the Dogubayazit fault (DF) passing to the north of the Dogubayazit city. In Iran, near the cities of Evoglou, Khadjimir and Qara-Ziaoddin, right-lateral slip on this fault displaces the course of the Qotourchai River and its tributaries—Aqchai, Qotourchai and Zilberchai (Fig. 9).

A system of faults forming a horsetail splay structure occurs on the northwestern flank of the Maku and Dogubayazit right-lateral strike–slip faults (Karakhanian et al., 2002). These splay faults have a normal fault component in addition to the right-lateral strike–slip. The largest and most typical is the Igdir fault (IF) that borders the Igdir depression from the west (Fig. 1). The horsetail splay fault system passes through the Greater and Lesser Ararat Volcanoes, and Aghri-Dag volcanic ridge, controlling the position of the principal volcanic eruption centers of Ararat and Aghri-Dag and forming a linear belt of parasitic volcanic cones (Karakhanian et al., 2002).

3.3. Gailatu–Siah Cheshmeh–Khoy fault system

Tchalenko (1977), Arpat and Iz (1977), and Barka and Kadinsky-Cade (1988) studied individual segments of the Gailatu, Siah Cheshmeh and Khoy faults; Berberian (1997) and Karakhanian et al. (1996) described them as a unified system.

The fault system trends N–NW and consists of en echelon segments. Near Lake Gailatu (Balikghel), the northwestern end of the fault forms a horsetail splay structure, with many faults having normal component (Fig. 1). To the southeast of Lake Gailatu, the GSKF system passes 10–20 km to the south of the Dogubayazit fault. There are four pull-apart basin-type structures along the GSKF: one in the region of Karakand village (Turkey), as well as three in Iran, near the towns of Kelissa-Kandi, Siah Cheshmeh and Zur Abad. These basins are 10–12 km long and up to 4–5 km wide each (Fig. 1), and depression flanks are accentuated by clearly developed young scarps. Normal fault scarps transverse to the principal fault direction cut the inner parts of the pull-apart depressions. The scarps are 10–15 m high, and this height is the observable part of the Holocene age vertical displacements. The height of the scarps decreases from east to west within the depressions. Along the edges of these pull-apart basins, there are right-lateral slip displacements of young ravines by 10–15 m and older ravines by up to 50 m. Creep-type offset of asphalt pavement and house fencing is evident in one of the streets in Siah Cheshmeh. Considering that the pavement was laid not earlier than 10 years ago and the vertical displacement amplitude of the street asphalt layer is 15 cm, the minimum possible vertical creep rate is 15 mm/year. Such high creep rates indicate high tectonic deformation of the fault in the last few years.

Westward from the city of Siah Cheshmeh, near the village of Isagulek, the Chalderan fault joins the GSKF (Berberian, 1997). In the southeast, the GSKF strikes toward the city of Khoy where it forms a large young depression and joins the North Mishu fault.

3.4. Hazard assessment

Historical and archaeological information records numerous natural disasters in the Ararat depression. At least three strong earthquakes ($M=6.0–7.0$) in the period of 851–893 AD are recorded on the Parackar–Dvin segment (PDF) (Shebalin et al., 1997). Earthquakes are known to have repeatedly destroyed Dvin, an ancient Armenian capital, killing several tens of thousands of people and forcing transfer of the capital to a new location.

There are no reliable data on strong historical seismicity on the Maku and Dogubayazit faults. Possibly, the 1843 Khoy earthquake ($M=5.9$) may be related to the Maku fault. In addition, the earthquake of 368 AD that destroyed Arshakavan (Dogubayazit), the capital of Armenian king Arshak the Second, may be associated with the Dogubayazit fault (Karakhanian, 1993; Haroutiunian et al., 1993; Guidoboni and Traina, 1995). A $M=5.2$ earthquake occurred on the Igdir fault (IF) in 1962. Since the Dogubayazit and Maku faults are 15–25 km north of the system of Gailatu–Siah Cheshmeh–Khoy fault, their involvement in past strong earthquakes must not be ruled out. Some of the strong events attributed to the Gailatu–Siah Cheshmeh–Khoy fault could equally occur on the Maku and Dogubayazit faults. These strong earthquakes include the events of 139 AD

Fig. 10. CORONA satellite image of the north part of the Ararat depression (see SF in Fig. 1). There are clearly visible offsets of historical riverbeds (1, 2, 3, 4 and 5) of the Arax River, migrating southward, due to the Sardarapat fault activity (SF).

(M=7.0), 1319 AD (M=7.4) and 1840 AD (M=7.4) (Ambraseys and Melville, 1982; Berberian, 1997; Karakhanian et al., 1997b).

River migration in response to tectonic, and possibly seismic, activation of faults contributes to natural hazards in the Ararat depression. The central

part of the Ararat depression accommodates a network of paleo-channels of the Arax River (Fig. 10). Vertical and horizontal displacements along the Sardarapat segment and the Sardarapat–Nakhichevan fault system have caused the Arax riverbed to migrate 12 km south. Bends and offsets of the abandoned paleo-channels confirm the right-lateral strike–slip activity of the Sardarapat fault (Fig. 10). Historical data allow estimation of the migration dates. In ancient times, the Arax River flowed along the foot of Davtiblour Hill (Fig. 10), and Armavir, the first capital of the Armenian Kingdom, was then situated there. According to the data of Movses Khorenatsi, an Armenian chronicler, the Arax River moved away from the city in 200–220 BC and since there was not enough water for the city and the king's court, the capital was moved to another location (Khorenatsi, 1990).

A later rearrangement of the river occurred along the Parackar–Dvin segment in 300–388 AD. At that time, Artashat, the Armenian capital, was situated at the confluence of the Arax with the Metsamor, another high-energy river. As a result of the activation of the Parackar–Dvin segment, flow on the Metsamor River ceased, and drainage split into five rivers (Sevjour, Kasakh, Hrazdan, Azat, and Vedi) that still today flow separately into the Arax River. The area around Artashat turned to marshes, and the air there filled with a stench, so King Khosrov Kotayk moved the capital to the city of Dvin (Khorenatsi, 1990).

Numerous paleo-channels of the Arax River can be traced in Turkish territory to the north and to the east of the city of Igdir. Modern migrations of the Arax River in 1931 and in 2001 have led to boundary disputes, since the border between Turkey and Armenia and between Iran and Azerbaijan is along this river.

Volcanic activity and landslides constitute other factors of natural hazard in this region. There is archaeological evidence for an eruption of pyroclastic flows from Ararat Volcano in 2500–2400 BC that destroyed a Koura–Arax culture settlement (Karakhanian et al., 2002). Historical sources indicate that volcanic activity on Ararat may also have occurred in the first half of the second century AD, the late third and early fourth centuries AD, and in 1450 and 1783 AD (Tiedeman, 1991; Karakhanian et al., 2002). Large earthquake-triggered landslides that caused casualties and destruction were recorded in the 139, 1319 and 1840 AD events (Karakhanian et al., 2000).

The 1840 Ararat earthquake provides the most comprehensive illustration of natural hazard potential in the Ararat depression. The $M = 7.4$ Ararat earthquake occurred on July 2, 1840 (Ambraseys and Melville, 1982). Areas around Ararat Volcano were destroyed totally, including many villages and cities of Dogubayazit, Maku, Ordoubad, Igdir, Kulp and Bazargan. The greatest destruction was reported for the western and southern flanks of the Ararat depression, but the northern and eastern parts were also damaged heavily. Up to 10,000 people died. The earthquake was accompanied by a gigantic landslide from the summit of Ararat (Stepanian, 1964; Ambraseys and Melville, 1982).

Our study of new historical data, particularly those from the archives of the Ararat Diocese of the Armenian Apostolic Church, reveals new eyewitness accounts of the earthquake in 1840 (Karakhanian et al., 2002), which mention the following key points.

1. Immediately after the main shock of the earthquake, a huge cloud resembling a smoke column rose over the canyon at the northern Ararat slope, where Akory village and St. Jakob's monastery were situated.
2. The inside of the cloud was illuminated with bright-red and blue light, while a strong acrid smell of sulfur was spreading around. Large stones, each weighing from 300–500 kg, were thrown up and out from a fissure upslope from the monastery and the village, landing at distances of 3–4 km. This was accompanied by sharp sounds in the canyon that resembled cannon gunnery.
3. The cloud rose up to the Ararat summit, and another cloud of dark red-luminous dust rolled down from the volcano summit at a great speed.
4. In moments, a dark fiery whirl of the cloud attacked the village of Akory, destroying it and killing 1900 of the villagers. The whirlwind had sufficient intensity to burn trees in the village gardens and pull them out with their roots. Shortly after that, the landslide reached the village and the monastery.
5. The landslide comprised blue liquid mud mixed with large stone blocks and moving at a great speed and with a strong smell. An airwave of huge speed and destructive force was moving ahead of

the flow front. The landslide flow exceeded a distance of 7 km and stopped at an elevation of 900 m above the Ararat valley level, forming a dam at the mouth of the Akory canyon. Large masses of semi-melted ice, mud, stones and water accumulated behind the dam.

6. The cloud, which rose from the Ararat summit, covered the sky and poured down with rain although the weather was clear.
7. Fields in the area of the falling rain were covered with a thick layer of liquid mud, dirt-blue in color and smelling harshly. Rainwater in pools was bright blue, resembling the color of vitriol.
8. Deep fractures formed in the Akory canyon after the earthquake: they were releasing turbid (vitriol) water of harsh sulfuric smell. Monks of the Echmiatsin monastery 55 km from Ararat also noticed a harsh smell of sulfur.
9. On July 6, 1840, at 7:00 a.m., a strong aftershock broke the landslide dam at the exit from Akory Canyon, and flows of melted ice, mud and stones flooded down again. Having covered a distance of 21 km at a great speed to reach the Arax river valley, the flows spread across a 12-km-wide front and solidified shortly after. The solidified deposits contained stone blocks and a thick layer of blue clay with pools of water of intense blue color. The flow-landslide destroyed the town of Aralik, several villages, and Russian military barracks, and dammed the Sevjour River.
10. Digging at the location of Akory village in 1840, Voskoboinikov found a thick layer of blue clay and stones covering the ruins of the village. The digs showed that the lower thirds of the walls had been preserved in all the houses, while timber roof slabs had been pressed into the floor by falling stones. According to Voskoboinikov, this proves that the village was ruined not by the rolling stones of the landslide, but rather by blocks falling vertically from above.
11. Describing the 1840 flow-landslide, Voskoboinikov in 1840, Abich in 1845 and Lynch in 1874 each provided drawings and photos of the flow deposits. According to their descriptions, the flow-landslide consisted of poorly cemented conglomerate with fragments of red-to-orange weathered volcanic rock, blue clay, mud and ice fragments.
12. In 1845 Abich identified a lengthy NW-striking fissure at the Greater Ararat summit, from which a smell of volcanic gases was felt strongly. Since preceding investigations of the Ararat summit by Parrot (1834) and Spassky-Antonov (1835) had contained no mention of that fissure, Abich considered it was an 1840 earthquake effect.

The analysis of the above accounts suggests that the 1840 ($M=7.4$) earthquake was accompanied by an explosive Bandai-type phreatic eruption from the northern slope close to the Ararat summit. The eruption produced an eruptive cloud rising to the Ararat summit (reports nos. 1, 2, 3, 6, 7 and 8) and pyroclastic flows that swept down on the Akory village (reports nos. 3, 4, 9, 11, and 12). Rittman (1964) also mentions an explosive gas eruption on Ararat in 1840 and the close similarity of that eruption to a Bandai-type eruption.

The 1840 eruption was accompanied by secondary volcanic effects. Eyewitnesses reported rain in the evening of July 2, a layer of blue liquid mud of harsh smell, and vitriol-blue water-pools left after the eruptive rain (reports nos. 7 and 8). Apparently, the debris flows (lahars) from the near-summit part of Ararat that flowed down the Akory canyon were another secondary phenomena accompanying the 1840 eruption. By our estimates, the volume of the 1840 Ararat debris flow was 3×10^8 m^3, and the speed was about 175 m/s. Reported descriptions of the debris flow (nos. 5, 9 and 11) suggest that the synchronous impacts of the explosive eruption and the earthquake destabilized and destroyed the upper slopes of Ararat. The detached part of the slope swept through the Akory canyon, breaking into pieces and gathering speed. Satellite images of the north slope of Ararat show clear traces of the 1840 flow and earlier debris flows.

In addition to eyewitness accounts, Major Voskoboinikov's (1840) data and Ambraseys and Melville (1982) confirm that the 1849 earthquake was accompanied by many other landslides in the areas of Pambouk and Chinghil (west of the Ararat depression) and Sharour and Zanghezour (north and east of the depression). The landslides buried the village of Karekh Khadjalou, causing the death of its population and cattle. In many places, the landslides dammed the Arax River, causing flooding across the neighborhood.

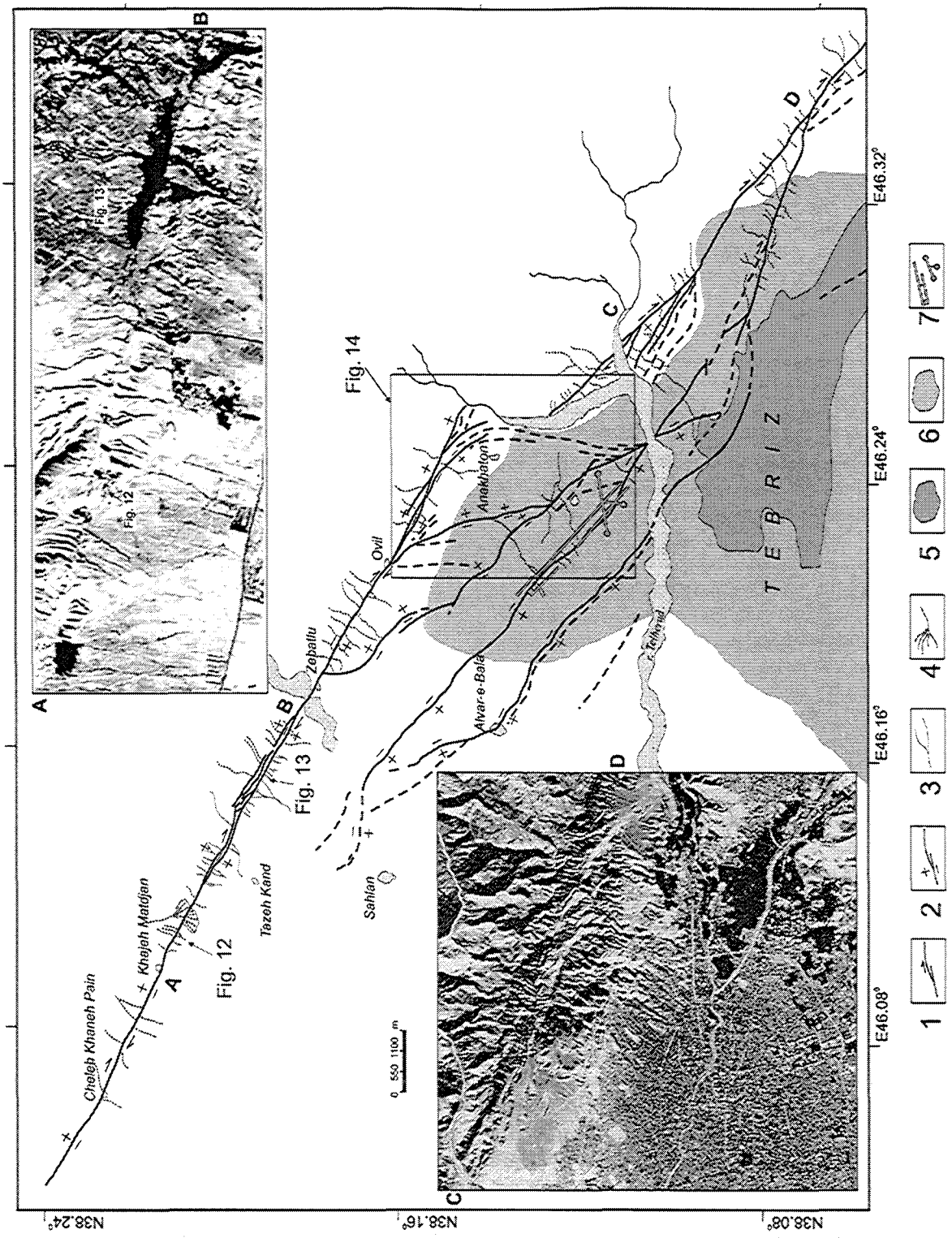
N38.24°
N38.16°
N38.08°
E46.08°
E46.16°
E46.24°
E46.32°
TEBRIZ
Chelgh Khaneh Pain
Khajeh Matdjan
Tazeh Kand
Sahian
Zebaltu
Ovil
Anakhaton
Alvar-e-Bala
Fig. 12
Fig. 13
Fig. 14
A
B
C
D
0 550 1100 m
1
2
3
4
5
6
7

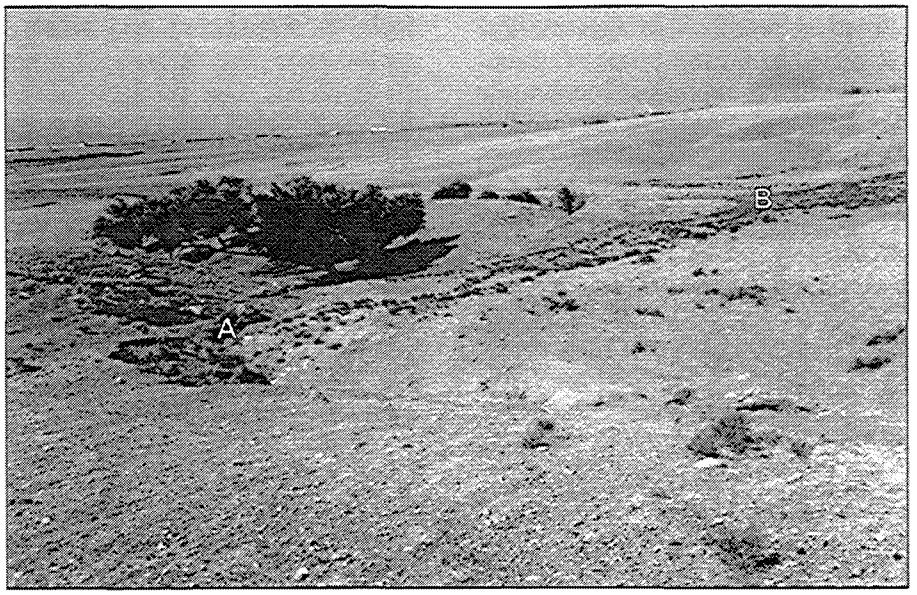

Fig. 12. Right-lateral offset of the river valley along the North Tabriz fault to the east of the village of Khajeh Mardjan; A–B–displacement amplitude.

In the central and northern parts of the Ararat depression, ground subsidence and extensive liquefaction formed along the riverbeds of Arax, Sevjour (Karassou), Akhourian and Arpa. The cracks in the ground were up to 4.5 m wide and formed wide belts more than 1 km long. A mixture of water, sand and large-size pebble was ejected from the cracks to the height of up to 1.5 m. The liquefaction destroyed the villages of Karakhasanlou, Alesher, Karachalou and several others.

In summary, in addition to the effects of seismic shaking, the earthquake of 1840 demonstrates how diverse natural hazards combine during a strong earthquake. Volcanic eruption, lahars, landslides, floods caused by river dams, ground subsidence and liquefaction, although all secondary to the earthquake, served to increase the damage and the number of casualties considerably. More than 4000 people out of the total death toll of 10,000 were killed by the secondary phenomena, and many populated areas were ruined by their joint impacts.

According to historical and archaeological data, strong earthquakes in the Ararat depression occurred between the eighth and second centuries BC, in 139, 368, 851–893, 1319 and 1840 AD (Stepanian, 1964; Ambraseys and Melville, 1982; Karakhanian, 1993; Haroutiunian et al., 1993; Berberian, 1994, 1997; Karakhanian et al., 2002). Volcanic eruptions from Ararat occurred in 2500–2400 and 550 BC and in 1840 AD; the migrations of the Arax and Metsamor Rivers took place in 200–220 BC and 300–388 AD; a large landslide from the summit of Ararat similar to the one in 1840 was recorded for the earthquake of 139 AD; many landslides accompanied the earthquakes of 893, 1319 and 1840 AD (Stepanian, 1964; Ambraseys and Melville, 1982; Karakhanian, 1993; Karakhanian et al., 2002).

Four ancient Armenian capitals situated in the Ararat depression were abandoned and moved to a new location in consequence of the mentioned impacts: Armavir in 220 BC, Arshakavan in 368 AD, Artashat in 388 AD and Dvin in 893 AD.

Fig. 11. Active faults in the Tabriz city region: AB and CD–Soviet system satellite image of the North Tabriz fault zone; 1–strike–slips; 2–vertical displacements: a–uplifted fault wall; b–downthrown fault wall; 3–river valleys and watercourses; 4–alluvial fans; 5–outline of the Tabriz city area in 1950 (city center); 6–outline of the Tabriz city area in 1996; 7–old and new Tabriz airports.

From the historical record, it is apparent that natural disasters caused by the integration of various natural phenomena during strong earthquakes are characteristic for the Ararat depression. The possible interaction between neighboring active fault systems in the Ararat depression (SF, PDF, NF, MF, DF, GSKF) may further increase the risk associated with the natural hazards.

4. Site 3: North Tabriz fault, city of Tabriz

Along the international border between NW Iran, eastern Turkey and south Armenia, there is quite a high level of seismic activity. Here, repeated strong earthquakes have destroyed many cities, most notably Tabriz in 1042 ($M=7.3$), 1641 ($M=6.8$), 1721 ($M=7.3$) and 1780 ($M=7.4$), Ararat in 1319 and 1840 (both $M=7.4$) and Chalderan in 1976 ($M=7.1$) (Ambraseys and Melville, 1982; Berberian, 1994, 1997; Berberian and Yeats, 1999). Historical data indicate that the maximum seismic hazard threatens the city of Tabriz. The high seismic hazard is linked to the activity of the North Tabriz fault, the North Mishu fault, the Tasuj fault and the Sufian fault. The information available on these faults is fragmentary and scanty. In 1996, we studied these four faults.

4.1. North Tabriz fault

Berberian (1997) divides the NTF into several segments that have a combined length of 210 km. The segments are identified according to a series of surface ruptures from the earthquakes of 1721, 1780 and 1786 AD. According to Berberian (1997), in the northwest, the NTF merges with a reverse fault zone that bends W–SW north of Lake Urmia (Fig. 1) (the Sufian and Tasuj faults); in the southeast, it merges into another zone of reverse faults that bends E–NE (South and North Bozqush, Duzduzan and South Sarab). On the Tabriz segment, Berberian (1976, 1997) observed vertical reverse-fault uplift of the northern side and inferred from air photo surveys signs of right-lateral strike–slip motion.

Our field studies of 1996 and our interpretation of satellite images indicated considerable strike–slip motions along the NTF. The geometry of the NTF zone is characterized by multiple right-stepping en echelon segments. Two fault segments, one to the west and one to the east of the Tabriz city, are of particular importance for seismic hazard assessment.

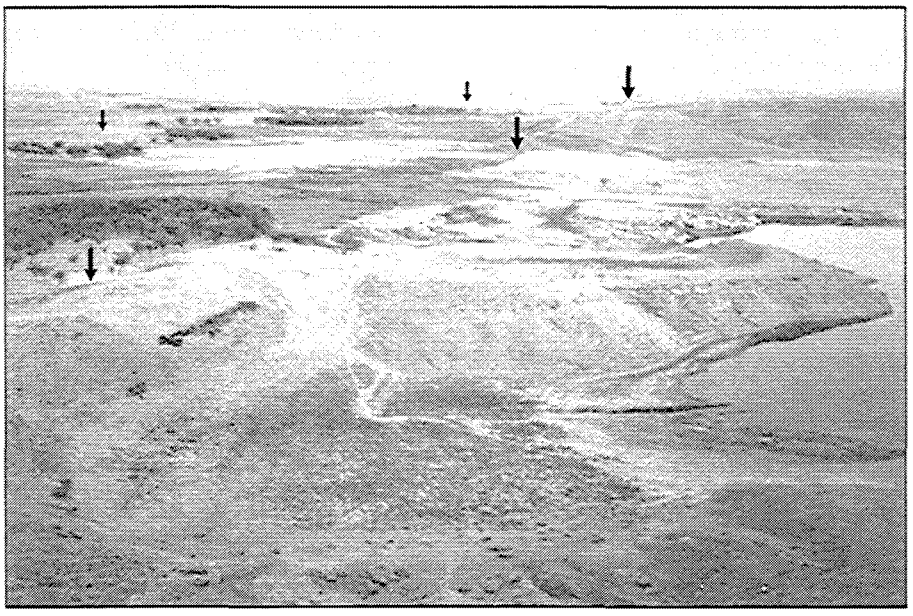

Fig. 13. Depression elongated along the North Tabriz fault (pull-apart basin) to the north of the village of Tazeh Kand.

The western fault segment strikes from Tabriz to the city of Sufian and bears clear signs of right-lateral strike–slip motions (Figs. 11 and 12). Right-slip amplitudes range from 100 m for large valleys (e.g., village of Zebarlu) to 25–30 m for young valleys (e.g., villages of Tazeh Kand, Ovil) to 3–5 m for minor streams (e.g., village of Khajeh Mardjan and Cheleh Khaneh Pain) (Figs. 11 and 12). The vertical displacements vary from 2–3 to 10 m, but are always between two and seven times less than the horizontal ones. The northern and southern sides of the en echelon segments are uplifted alternately, a typical characteristic of strike–slip faults (Fig. 13). Small pull-apart depressions are formed at the sites of fault segment overlap (e.g., village of Tazeh Kand, Figs. 11 and 13). To the east of the village of Khajeh Mardjan, the NTF separates the Upper Red Formation of a Miocene age in the north from Quaternary deposits in the south. Small gullies of probable late Holocene age are right-laterally displaced by 8 m along the main branch of the fault. This observation leads to a very rough estimation of the minimum slip rate on this fault

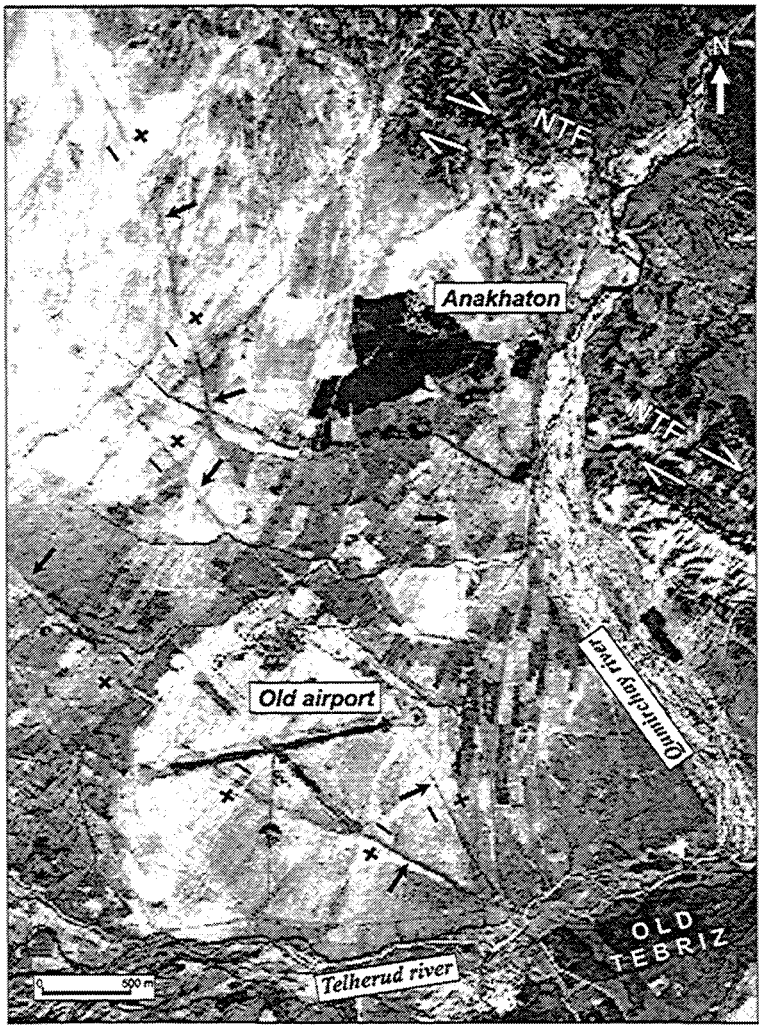

Fig. 14. An air photo of 1955 (no. 1875) for the area surrounding the Tabriz airport; the arrows indicate NW-branching young ruptures, which display right-lateral strike–slip motions and form a stepwise low to the center of the Tabriz pull-apart. Apparently, these are the ruptures of the $M=7.4$ earthquake in 1780 and of earlier events.

segment, which is at least 1.5–2 mm/year (Karakhanian et al., 1996).

The eastern segment is shifted southwards with respect to the western one and strikes from the city of Tabriz to the village of Basmedge. These two segments define the intervening Tabriz pull-apart basin (Fig. 11). Young ruptures on the flanks of both segments branch in a NW direction and have right strike–slip offsets, which form a graben-shaped stepped depression in the center of the pull-apart. These young ruptures have clear scarps and can be traced through the northern part of the city of Tabriz. Today, these scarps cross the runways of the old and new Tabriz airports and the new highway line (Figs. 11 and 14). Apparently, these are seismogenic surface ruptures produced by the 1780 (M=7.4) earthquake and by earlier events, which are clearly visible on the 1955 air photo (no. 1875) (Fig. 14).

4.2. North Mishu fault

The western continuation of the North Tabriz fault is the North Mishu fault (NMF). This 80-km-long fault consists of two segments, of which the western segment stretches from the village of Dizajbiz to the village of Baghlar, while the eastern one (actually called the North Mishu fault) extends from Baghlar to the city of Sufian (Fig. 1).

The eastern NMF segment is much more active than the western one, with young right strike–slip offsets of river valleys evident along it. Multiple fault scarps in the NMF zone may be related to the historical earthquakes of 1780 (M=7.4) and 1786 (M=6.3). The maximum and minimum right-lateral offsets for the largest and the smallest of the scarps are 10 and 1–3 m, respectively. The vertical displacements are 2–3 m on average and are represented by reverse faults with the uplifted southern wall and the slip plane dipping to the south at 70–80°. The dextral strike–slip displacements are clearest in the region of the villages of Payam, Baghlar and Sivan, but are largest (up to 250 m) to the south of the village of Sivan.

4.3. Hazard assessment

Many strong historical earthquakes were recorded along the North Tabriz and North Mishu faults (Ambraseys and Melville, 1982; Berberian, 1994, 1997). All these earthquakes caused rather heavy damage to the city of Tabriz. The earthquakes of 1042 (M=7.3) and 1721 (M=7.3) alone killed about 40,000 of people each, while more than 50,000 died during the event of 1780 (M=7.4) (Ambraseys and Melville, 1982; Berberian, 1994, 1997). The earthquakes were often accompanied by large landslides, extensive liquefaction and lengthy surface ruptures. According to Ambraseys and Melville (1982) and Berberian (1997), the SE Shebli segment of the NTF had ground breaks of 50–35 km during the 1721 (M=7.3) earthquake, and the NW Tabriz segment ruptured for 45–42 km, with a vertical displacement of 2–4 m, during the event of 1780 (M=7.4). Berberian (1997) describes earthquakes clustering in time along the NTF, the first cluster including three strong earthquakes in 1721–1786, and the second including two events of 1273 and 1304.

One important fact for the seismic hazard assessment is that the North Tabriz fault, North Mishu fault and Gailatu–Siah Cheshmeh–Khoy fault are contiguously linked with each other, to form a single 550-km-long system of the North Tabriz–Gailatu fault (NTGF, Fig. 1). This fault system controls the main seismic hazard in the territory of NW Iran, SE Turkey and partly southern regions of Armenia and Azerbaijan. The zone of strong seismic impact from the North Tabriz–Gailatu fault includes the large cities of Maku, Khoy, Marand, Sufian and Tabriz, numerous villages in NW Iran, as well as the cities of Dogubayazit, Igdir and numerous villages in SE Turkey. Cities and villages in Nakhichevan (Azerbaijan), including Nakhichevan and Ordoubad, and in Armenia (Artashat, Yerevan, Armavir, Metsamor and others) fall in the zone of more moderate seismic impact.

A distinct episode of 60-year periodicity of strong earthquakes along the system of North Tabriz–Gailatu fault system is of particular interest. The SE segment of this system (Tabriz–Shebli NTF segment) ruptured in 1721 (M=7.3). Fifty-nine years later, the 1780 (M=7.4) event produced rupture on the central segment (NTF segments, Tabriz–Sufian and North Mishu faults), and 60 years after that, the NW segment (GSKF) ruptured in the event of 1840 (M=7.4).

The North Tabriz–Gailatu fault system poses particularly high hazard for the city of Tabriz for the following reasons.

1. Tabriz is in the system of North Tabriz–Gailatu fault, which has 12 historical earthquakes of $M=6.2–7.4$ on the NTF segments within 960 years (from 858 to 1819). The earthquakes caused severe destruction in the city, killed more than 130,000 people and produced surface ruptures that pass beneath the NW part of the modern city, airport area, highway and railway lines (Figs. 11 and 14).
2. There are weak soils and landslide-prone areas in the city.
3. There are creep-like motions (at the rate of 15 mm/year) on the western NTGF segment, weak and medium-size seismicity on the western and central segments of the NTGF in contrast to the seismic quiescence on the eastern flank (NTF) in the Tabriz city region. An important note is that, as of today, the strong earthquake quiescence period has already lasted for more than 200 years, which can be considered a factor increasing the threat.

All these factors together make Tabriz (a city with the population of 1.2 million) one of the most seismically hazardous cities of the world, with high probability of strong earthquake on the eastern flank of the NTGF in near future. Since the North Tabriz–Gailatu fault system also poses a high seismic hazard to the adjacent territories of NW Iran, SE Turkey, Nakhichevan (Azerbaijan) and southern Armenia, it therefore requires further study.

5. Discussion

Seismic hazard assessment is a particularly difficult task for countries facing severe social and economic problems. In many cases, strong earthquakes unexpectedly surpass the anticipated hazard parameters and lead to the reassessment of the seismic hazard level. For the period from 1948 to 1995, nine strong earthquakes in the USSR and CIS each compelled considerable revision and increase of the seismic hazard estimates (Arefiev, 2001). The same happened after strong earthquakes in Armenia (Spitak, 1988), Turkey (Chalderan, 1976; Izmit, 1999) and Iran (Roudbar, 1990).

As a rule, natural hazard and risk assessment studies pay most attention to the impacts of strong seismicity. However, seismic effects may be considerably enhanced by other accompanying natural phenomena (volcanic eruptions, lahars, landslides, floods and river migrations). Generally, these natural hazards are studied by different disciplines separately, and the results, as a rule, are never integrated in natural hazard assessments.

As shown by the examples considered above, the hazardous phenomena that are secondary with respect to strong seismicity may cause the largest figures of casualties and material losses and thus constitute an essential component of the natural risk factor.

Although the Pambak-Sevan-Sunik and Garni faults are characterized by low slip rates (0.5–4 mm/year) and no high seismic potential has been associated with them, our paleoseismological studies provide new evidence that reveals a large number of previously unreported strong earthquakes ($M \sim 7.2–7.4$) in these fault zones (Tables 2 and 3).

The paleoseismological studies in the GF zone, along the surface rupture of the 1988 Spitak earthquake ($M_s=7.1$), identified one $M>7.1$ event that occurred after 21,274–20,519 years BP (1σ) (17,565 ± 170 years BP) and one $M>7.0$ event after 24,765 ± 770 years BP (Philip et al., 1992; Karakhanian et al., 2002). This yields 20,000 years of the maximum recurrence interval between the last events, assuming no seismic events have been missed. Eight earthquakes of $M \geq 6.7–7.4$ have been identified on individual segments of the Pambak-Sevan-Sunik fault, with an average recurrence interval for $M>7.0$ earthquakes ranging from 2000 to 4000 years (Philip et al., 2001; Avagyan, 2001; Karakhanian et al., 2002).

Therefore, $M=7.0–7.4$ earthquakes on the low slip-rate faults (0.5–4 mm/year) in the center of the Arabian collision zone can recur at rather long intervals varying from 2000 to 20,000 years. This is an important factor to consider in seismic hazard assessments for areas, where low slip rates on active faults and an absence of long-term seismic history do not suggest any potential of $M>7.0$ earthquakes.

Interaction of closely spaced active faults during strong earthquakes is an important factor that increases

seismic hazard in the considered regions. The 1988 Spitak earthquake, for instance, was confined to the junction of four active faults, the two of them (PSSF and GF) having right strike–slip motion, and the other two (ESF and AF) having left strike–slip motion. The Spitak earthquake had five sub-sources separated in space and time (Dorbath et al., 1992). Surface ruptures from the Spitak earthquake reactivated diverse active faults: a 32-km-long right-slip with reverse component on the GF; a 300-m-long right-slip on the PSSF1 and 500-m-long left strike–slip on the ESF (Philip et al., 1992; Trifonov et al., 1990; Karakhanian, 1992; Karakhanian and Balassanian, 1992). Such a complex seismotectonic setting of the source ensured the extended duration of the main shock, which lasted for more than 3 min; it also increased its spatial dimensions, which in turn increased the destruction and enlarged the affected area considerably. Apparently, a similar complex source model can be suggested for a series of historical earthquakes, among them the 1139 Gandzak, 1679 Garni and 1840 Ararat events.

Formation of horsetail splay structures and pull-apart basins in active fault zones can complicate seismic hazard assessment. The paleoseismological investigation on the 1988 Spitak rupture revealed two events of $M=7.1-7.2$ separated by an interval of several thousand years; one occurred after cal. 21,274–20,519 years BP by 1σ ($17{,}565 \pm 170$ years BP) and the other after $24{,}765 \pm 770$ years BP (Philip et al., 1992). It is probable that strong earthquakes would have occurred on the neighboring branch of the horsetail splay structure in the time interval separating the two events on the 1988 Spitak rupture. A similar pattern may characterize the two branches of seismogenic ruptures in the Fioletovo depression. In this depression, the PSSF2 and PSSF1 segments overlap; trenching at site 5 (Fig. 2; Tables 1 and 2) revealed two surface ruptures that formed around 2200 BC (Philip et al., 2001). Triggering of one of these events with the other occurring on the neighboring segment (PSSF2 and PSSF1) must not be ruled out. Two other paleo-ruptures were revealed in a trench on the PSSF2 segment, 400 m south of site 5; one of these ruptures is predated, and the other postdated by a calibrated estimate of 9489–7588 years BP (1σ) (Philip et al., 2001).

Therefore, each fault branch in the horsetail splay structures and pull-apart basins can generate strong earthquakes. Such a tendency must be considered in the assessment of earthquake recurrence period, maximum credible earthquake and slip rates, assuming that it may increase seismic hazard due to the potential triggering of earthquakes by several sub-sources as in the case of the 1988 Spitak event and, possibly, of the two paleo-events around 2200 BC.

Clustering of strong earthquakes along one or several linked active faults is an additional factor of seismic hazard characteristic of the considered areas. Historical evidence indicate that there were several cases of earthquake clustering on the North Anatolian fault similar to the cluster of events recorded there in the middle of the 20th century (Trifonov et al., 1994). Clustering of strong historical earthquakes is identified for the Eastern Anatolian, Levant, North Tabriz, Dogubayazit and other faults (Trifonov et al., 1994; Berberian, 1997, 1999; Karakhanian et al., 2002). From the southeast to the northwest along the Garni fault zone, six earthquakes occurred in sequence: 368 ($M=7.0$), 735 ($M=7.2$), 906 ($M=6.8$), 1679 ($M=7.1$), 1827 ($M=6.8$) and 1988 ($M=7.0$) (Karakhanian et al., 2002). Clustering of seismic events has been established for the paleo-events on the Pambak-Sevan fault and for the fault system of Gaulatu-Siah Cheshmeh–Khoy–North Tabriz.

An important fact to consider assessing seismic hazard is the alternation of long-term quiescence with periods of abrupt activation of strong seismicity, manifested in clustering of several earthquakes in space and time. A long pause in strong seismicity preceded the familiar cluster of strong earthquakes that migrated along the North Anatolian fault in the 20th century. Similar patterns have been observed for individual faults in the central part of the collision. In the south of Armenia, for instance, the Parackar–Dvin fault, after being quiet for a long time, reactivated with a cluster of several strong ($M=6.5-7.0$) earthquakes within 42 years (from 851 to 893 AD). One after another, each of those events razed Dvin, an ancient Armenian capital, to the ground. Since then, the fault has been quiet and has not been generating strong earthquakes for 1100 years (till the present).

Many of the strong earthquakes in the study region triggered large landslides (Karakhanian et al., 2000). In areas such as the Vanadzor depression, such landslide hazards can drastically enhance destructive earthquake impacts and change the seismic hazard estimate. A

similar enhancement can be made when volcanic eruptions are induced by strong seismicity. A modern example of such a seismo-volcanic interaction was the Ararat volcano eruption during the 1840 AD earthquake (Karakhanian et al., 2002). Eruptions during strong earthquakes were reported for the following volcanoes: Nemrout and Tondourek, 1692 and 1881 AD, respectively (Turkey), as well as in the SE Turkey and north Syria in 499–502 AD, south Turkey in 520–521, 715 and 1050–1053 AD (Karakhanian et al., 2002).

Although the link between tectonic and volcanic activity is commonly accepted, many structural and chronological manifestations of this association in the Arabian zone of continental collision are still insufficiently studied. Extensive development of young volcanism in a continental shortening area with predominant compressive stress field is paradoxical both in structural and geodynamic respect and calls for careful study. The link between tectonic, seismic and volcanic activation is of particular interest. In most of the cases, the volcanic activity resulted from tectonic and seismic activation of faults. A series of publications describe the possibility of such causal correlation (Doumas, 1990; Hill et al., 1993; Guidoboni et al., 1994; Karakhanian et al., 1997a). Some of the volcanoes in the studied regions are located inside pull-apart basins and controlled by active faults. Tectonic stresses that accumulate in the pull-apart basins are released as strong earthquakes forming large seismogenic surface ruptures. Penetrating into magma sources, the ruptures may cause volcanic eruptions.

In summary, seismic activation serves as a triggering mechanism for a number of interrelated natural hazards. Strong earthquakes, volcanic eruptions, landslides, soil effects, floods and river migrations integrate to form a single-whole complex of natural hazards (Trifonov, 1990). Each of the hazards alone may not reach the level hazardous for people, but acting together, they can cause a disaster.

Study of this relationship and integration as natural hazard and risk factor is of importance for Armenia, eastern Turkey, western Iran and adjacent countries. Mostly, this concerns the areas of state border junction. The transboundary character of active faults requires transboundary cooperation in their study, as well as in the assessment and reduction of the natural risk.

Acknowledgements

This research was possible thanks to the funding under the following grants: PICS-417, NATO EST. CLG 977044, UNDP, INTAS 0840 and ISTC A-651 KCAUSIN. The authors are grateful to Dr. J.L. Michelot (Laboratory of Hydrology and Isotopic Geochemistry, Paris Sud University) and Dr. L.D. Sulerzhitsky (Geological Institute of the Russian Academy of Sciences) for the radiocarbon dating of samples, Dr. M. Ghafory-Ashtiany and Dr. M. Abbasi for their help and support in the organization of field works in Iran (International Institute of Earthquake Engineering and Seismology, Tehran), Dr. Ruben Badalyan and Dr. Pavel Avetissyan (Institute of Archaeology and Ethnography of the National Academy of Sciences, Yerevan, Armenia) for their inestimable help and support to the implementation of this work. Field investigations were carried out while F. Jamali was working for the International Institute of Earthquake Engineering and Seismology, Tehran, Iran. The authors are grateful to Dr. I. Stewart for helpful comments and to Y. Abgarian for contribution to the preparation of the manuscript.

References

Ambraseys, N.N., Jackson, J.A., 1998. Faulting associated with historical and recent earthquakes in the Eastern Mediterranean region. Geophys. J. Int. 133, 390–406.

Ambraseys, N.N., Melville, C.P., 1982. A History of Persian Earthquakes. Cambridge Univ. Press, New York, p. 219.

Arefiev, S.S., 2001, Epicentral observations and geodynamic source models of strong earthquakes. Abstract of the Thesis, Moscow, p. 56.

Arpat, E., Saroglu, F., Iz, H.B., 1977. The 1976 Caldiran earthquake. Yeryuvari Insan 2, 29–41.

Avagyan, A., 2001. Estimation of slip rates and recurrence intervals of strong earthquakes on the fault system of Pambak-Sevan-Sunik (Armenia): segmentation and relation with volcanic activity. PhD Thesis, Montpellier II University, France, p. 180.

Barka, A.A., Kadinsky-Cade, K., 1988. Strike–slip fault geometry in Turkey and its influence on earthquake activity. Tectonics 3, 663–684.

Berberian, M., 1976. Contribution to the seismotectonics of Iran. Part II. GSI Report 39, 516.

Berberian, M., 1981. Active faulting and tectonics of Iran. Zagros–Hindu Kush–Himalaya Geodynamic Evolution. In: Gupta, H.K., Delany, F.M. (Eds.), Am. Geophys. Union, Geodyn. Ser. vol. 3, pp. 33–69.

Berberian, M., 1994. Natural hazards and the first catalogue of Iran. Historical hazards in Iran prior to 1900. International Institute of Earthquake Engineering and Seismology, vol. 1. Tehran, Iran, p. 603.

Berberian, M., 1997. Seismic sources of the Transcaucasian historical earthquakes. In: Giardini, D., Balassanian, S. (Eds.), Historical and Prehistorical Earthquakes in the Caucasus. Kluwer Academic Publishing, Dordrecht, Netherlands, pp. 233–311.

Berberian, M., Yeats, R.S., 1999. Patterns of historical earthquake rupture in the Iranian Plateau. Bull. Seismol. Soc. Am. 89, 120–139.

Birbrayer, A.N., Krasenkov, N.D., 1973. Dynamic calculation of slope stability considering potential dislocation. Trudi Koordinacionnogo Soveschania po Gidrotekhnike, issue 80. Dynamic Properties of Soils and Earthquake Resistance of Hydroengineering Structures. Energia Publishing House, Leningrad, pp. 35–41 (in Russian).

Chase, C.G., 1978. Plate kinematics: the Americas, East Africa, and the rest of the world. Earth Planet. Sci. Lett. 37 (3), 355–368.

Davies, T.R.H., 1982. Spreading of rock avalanche debris by mechanical fluidization. Rock Mech. 15, 9–24.

De Mets, C., Codon, R.G., Argus, D.F., Stein, S., 1990. Current plate motion. Geophys. J. Int. 101, 425–478.

Dewey, J.F., Hempton, M.R., Kidd, W.S.F., Saroglu, F., Sengor, A.M.C., 1986. Shortening of continental lithosphere: the neotectonics of Eastern Anatolia—a young collision zone. In: Coward, M.P., Riea, A.C. (Eds.), Collision Tectonics. Geol. Soc. Lond., Spec. Publ., vol. 19, pp. 3–36.

Dorbath, L., Dorbath, C., Rivera, L., Fuenzalida, A., Cisternas, A., Tatevossian, R., Aptekman, J., Arefiev, S., 1992. Geometry, segmentation and stress regime of the Spitak (Armenia) earthquake from the analysis of the aftershock sequence. Geophys. J. Int. 108, 309–328.

Doumas, C., 1990. Archaeological observations at Akrotiri related to the volcanic destruction, Thera and the Aegean World III, 3, Chronology. Proc. of the 3rd International Congress, Santorini, Greece. The Thera Foundation, London, pp. 48–50.

Guidoboni, E., Traina, G., 1995. A new catalogue of earthquakes in the historical Armenian area from antiquity to the 12th century. Ann. Geofis. 38 (1), 85–147.

Guidoboni, E., Comastri, A., Traina, G., 1994. Catalogue of Ancient Earthquakes in the Mediterranean Area up to the 10th Century. Istituto Nazionale di Geofisica, Rome, p. 504.

Guidoboni, E., Traina, G., Dorfmann, I., Kldiashvili, D., 1996. Catalogue of Earthquakes in Armenia in the 13th–18th Centuries. Storia Geofisica Ambiente, Bologna.

Hanks, T.C., Kanamori, H., 1979. A moment magnitude scale. J. Geophys. Res. 84, 2348–2350.

Haroutiunian, R.A., Karakhanian, A.S., Assatrian, A.O., 1993. Unknown historical earthquakes of the Armenian Upland. Abstracts Int. Conf. on Continental Collision Zone Earthquakes and Earthquake Hazard Reduction. National Survey of Seismic Protection, Yerevan, Armenia, pp. 35–36.

Hill, D.P., Reasenberg, P.A., Michael, A., Arabaz, W.J., Beroza, G., Brumbaugh, D., Brune, J.N., Castro, R., Davis, S., de Polo, D., Ellsworth, W.L., Gomberg, J., Harmsen, S., House, L., Jackson, S.M., Johnston, M.J.S., Jones, L., Keller, R., Malone, S., Munguia, L., Nava, S., Pechmann, J.C., Sanford, A., Simpson, R.W., Smith, R.B., Stark, M., Stickney, M., Vidal, A., Walter, S., Wong, V., Zollweg, J., 1993. Seismicity remotely triggered by the magnitude 7.3 Landers, California, earthquake. Science 260, 1617–1623 (June 11).

Jackson, J., McKenzie, D.P., 1988. The relationship between plate motions and seismic moment tensors, and the rates of active deformation in the Mediterranean and Middle East. Geophys. J. 93, 45–73.

Jibson, R.W., 1996. Use of landslides for paleoseismic analysis. Eng. Geol. 43, 291–323 (Elsevier).

Jibson, R.W., Prentice, C.S., Borissoff, B.A., Rogozhin, E.A., Langer, C.J., 1994. Some observations of landslides triggered by the 29 April 1991 Racha Earthquake, Republic of Georgia. Bull. Seismol. Soc. Am. 84 (4), 963–973.

Karakhanian, A., 1993. The active faults of the Armenian Upland. Proc. of the Scientific Meeting on Seismic Protection. Dipartamento per la Geologia e le Attivita estrattive, Regione del Veneto, Venice, Italy, pp. 88–94.

Karakhanian, A.S., 1992. Some features of active tectonics in the 1988 Spitak earthquake zone. Izvestia AN Armenii, Nauki o zemlie 1, 3–11 (in Russian).

Karakhanian, A.S., Balassanian, V.S., 1992. Active dynamics of the 1988 Spitak earthquake zone. Izvestia AN Armenii, Nauki o Zemlie 2, 12–21 (in Russian).

Karakhanian, A., Jamali, F.H., Hessami, K.T., 1996. An investigation of some active faults in the Azarbaidjan region (NW Iran). Report IIEES. Tehran, 7.

Karakhanian, A.S., Trifonov, V.G., Azizbekian, O.G., Hondkarian, D.G., 1997a. Relationship of the late Quaternary tectonics and volcanism in the Khonarassar active fault zone, the Armenian Upland. Terra Nova 9, 131–134.

Karakhanian, A.S., Djrbashyan, R.T.,, Trifonov, V.G., Philip, H., Ritz, J.F., 1997b. Active faults and strong earthquakes of the Armenian Upland. In: Giardini, D., Balassanian, S. (Eds.), Historical and Prehistorical Earthquakes in the Caucasus. Kluwer Academic Publishing, Dordrecht, Netherlands, pp. 181–187.

Karakhanian, A., Bagdassarian, H., Arakelian, S., Avagyan, A., Davtian, V., Adilkhanian, A., Balassanian, V., Abgaryan, Y., 2000. Landslide Hazard and Risk: Geographic Information System on Landslide Hazard and Risk Assessment in the Republic of Armenia. UNDP, Yerevan, p. 274.

Karakhanian, A., Djrbashian, R., Trifonov, V., Philip, H., Arakelian, S., Avagian, A., 2002. Holocene-historical volcanism and active faults as natural risk factor for Armenia and adjacent countries. J. Volcanol. Geotherm. Res. 113 (1–2), 319–344.

Keefer, D.K., 1994. The importance of earthquake-induced landslides to long-term slope erosion and slope-failure hazards in seismically active regions. Geomorphology 10, 265–284 (Elsevier).

Khachiyan, E. (Ed.), 1998. SNPA II-2.02.-94, Building Code of the Republic of Armenia, Earthquake Engineering Code 1998.

Official Publishing House of the Urban Development Ministry of the Republic of Armenia, Yerevan, p. 42.

Khorenatsi, 1990. History of Armenia, Translation From Ancient Armenian and Comments by G. Sarkissian. Publishing House Hayastan, Yerevan, Armenia, p. 291.

Kondorskaya, N.V., Shebalin, N.V. (Eds.), 1980. Seismic Zoning of the USSR Territory. Nauka, Moscow, 307 pp. (in Russian).

McCalpin, J.P., Nelson, A.R., 1996. Introduction to paleoseismology. In: McCalpin, J.P. (Ed.), Paleoseismology. International Geophysics Series, vol. 62. Academic Press, San Diego, CA, p. 588.

Minster, J.B., Jordan, T.H., 1978. Present-day plate motions J. Geophys. Res. 83, 5331–5354.

Nikonov, A., Nikonova, K., 1986. The strongest earthquake in the Transcaucasus, September 30, 1139. Voprosi Ingenernoj Seismologii, vol. 27. Nauka, Moscow, pp. 152–183 (in Russian).

Parrot, F., 1834. Reize zum Ararat. Theil, Haude und Spenerschen, Berlin, p. 231.

Philip, H., Karakhanian, A., 1999. Treblements de terre et archeologie. Pour Sci. (edition Francaise de Scientific American), 36–40 (July).

Philip, H., Cisternas, A., Gvishkiani, A., Gorshkov, A., 1989. The Caucasus: an actual example of the initial stages of continental collision. Tectonophysics 161, 1–21.

Philip, H., Rogozhin, E., Cisternas, A., Bousguet, J.C., Borisov, A., Karakhanian, A.S., 1992. The Armenian earthquake of 1988 December 7: faulting and folding, neotectonics and paleoseismicity. Geophys. Int. J. 110, 141–158.

Philip, H., Avagyan, A., Karakhanian, A., Ritz, J.-F., Rebai, S., 2001. Slip rates and recurrence intervals of strong earthquakes along the Pambak-Sevan-Sunik fault (Armenia). Tectonophysics 343 (3–4), 205–232.

Rebai, S., Philip, H., Dorbath, L., Borissoff, B., Haessler, H., Cisternas, A., 1993. Active tectonics in the Lesser Caucasus: coexistence of compressive and extensional structures. Tectonics 12 (5), 1089–1114.

Reilinger, R., Barka, A., 1997. GPS constraints on fault slip rates in the Arabia–Africa–Eurasia plate collision zone: implications for earthquake recurrence times. In: Giardini, D., Balassanian, S. (Eds.), Historical and Prehistorical earthquakes in the Caucasus, ILP publication 333, vol. 28. Kluwer Academic Publishing, Dordrecht, Netherlands, pp. 91–108. NATO ASI Series.

Rittman, A., 1964. *Volcanoes and Their Activity.* Mir Publishing House, Moscow, p. 436 (in Russian).

Seismic Hazard Assessment for the Areas of Vanadzor Chemical Plant CJSC and Vanadzor TPP SCJSC, 1999. NSSP Report, Yerevan, p. 87.

Shebalin, N.V., Nikonov, A.A., Tatevosian, R.E., Mokrushina, N.G., Petrossian, A.E., Kondorskaya, N.V., Khrometskaya, E.A., Karakhanian, A.S., Harutunian, R.A., Asatrian, A.O., Piruzian, S.A., Gassanov, A.G., Varazanashvili, O.D., Papalashvili, V.G., Golinskiy, G.L., Karryev, B., Pustovitenko, B.G., Kulchtiskiy, V.E., 1997. Caucasus test-area strong earthquake catalogue. In: Giardini, D., Balassanian, S. (Eds.), Historical and Prehistorical Earthquakes in the Caucasus. Kluwer Academic Publishing, Dordrecht, Netherlands, pp. 210–223.

Shoja-Taheri, J., Niazi, M., 1981. Seismicity of the Iranian Plateau and bordering regions. Bull. Seismol. Soc. Am. 71, 477–489.

Slemmons, D.B., 1982. Determination of design earthquake magnitudes for microzonation. Proceedings of the 3rd International Earthquake Microzonation Conference, vol. 1. University of Washington, Seattle, WA, pp. 119–130.

Spassky-Antonov, K., 1835. Ueber eine newe Besteigung des Ararat, August 1834. Magazin fur die Literatur des Auslandes 34, 76 (Berlin).

Stepanian, V.A., 1964. The earthquakes in the Armenian upland and the surrounding region. Haiastan, Yerevan, 342 pp. (in Armenian).

Stuiver, M., Reimer, P.J., 1993. Radiocarbon 35, 215–230.

Taymaz, T., Eyidogan, H., Jackson, J., 1991. Source parameters of large earthquakes in the East Anatolian fault zone (Turkey). Int. Geophys. J. 106, 537–550.

Tchalenko, J.S., 1977. A reconnaissance of seismicity and tectonics on the northern border of the Arabian plate (Lake Van region). Rev. Geogr. Phys. Geol. Dyn. 19, 189–208.

Tiedeman, H., 1991. Catalogue of Earthquakes and Volcanic Eruptions. Swiss Re, Zurich, p. 94.

Trifonov, V.G., Karakhanian, A.S., Kozhurin, A.I., 1990. The Spitak earthquake as a manifestation of active tectonics. Geotectonika 6, 46–60 (in Russian).

Trifonov, V.G., 1990. Natural disasters in the system of recent geodynamic processes. Recent Geodynamics and Deep Structure of the Territory of the USSR. Nauka Press, Moscow, pp. 111–116 (in Russian).

Trifonov, V.G., Karakhanian, A.S., Kozhurin, A.J., 1994. Major active faults of the collision area between the Arabian and the Eurasian plates. Proc. of the Conference on Continental Collision Zone Earthquakes and Seismic Hazard Reduction. IASPEI/IDNDR, Yerevan, pp. 56–79.

Trifonov, V.G., Karakhanian, A.S., Berberian, M., Ivanova, T.P., 1996. Active faults of the Arabian Plate bounds, Caucasus and Middle East. J. Earthq. Predict. Res. 5 (3), 363–374.

Voskoboinikov, 1840. Report to General Golovin (paragraph 496 of 25.11.1840, 210), Deeds collected by the Caucasian Archaeological Commission, Archive of the Caucasian Governor's Principal Administration, vol. 9. Tiflis, p. 580.

Wells, D.L., Coppersmith, K.H., 1994. Empirical relationships among magnitude, rupture length, rupture area, and surface displacement. Bull. Seismol. Soc. Am. 84, 974–1002.

Working Group on California Earthquake Probabilities, 1988. Probability of large earthquakes occurring in California on the San Andreas fault. U.S. Geol. Surv. Open-File Rep. 88-398, 1–62.

Yeats, R.S., Sieh, K., Allen, C.R., 1997. The Geology of Earthquakes. Oxford Univ. Press, Oxford, NY.

Yilmaz, V., Guner, Y., Saroglu, F., 1998. Geology of the quaternary volcanic centers of the East Anatolia. J. Volcanol. Geotherm. Res. 85 (1–4), 173–210.